Lh. 2066

LMSC-D-766341

MASTER

CADMIUM SULFIDE/COPPER SULFIDE HETEROJUNCTION CELL RESEARCH

Final Report, February 26, 1979—May 31, 1980

By
W. W. Anderson
A. D. Jonath

June 1980

Work Performed Under Contract No. AC02-77CH00178

Lockheed Palo Alto Research Laboratory
Lockheed Missiles & Space Company, Inc.
Palo Alto, California

DIST-278
NTIS-25

U.S. Department of Energy

R101

Solar Energy

DISTRIBUTION OF THIS DOCUMENT IS UNLIMITED

DISCLAIMER

This report was prepared as an account of work sponsored by an agency of the United States Government. Neither the United States Government nor any agency thereof, nor any of their employees, makes any warranty, express or implied, or assumes any legal liability or responsibility for the accuracy, completeness, or usefulness of any information, apparatus, product, or process disclosed, or represents that its use would not infringe privately owned rights. Reference herein to any specific commercial product, process, or service by trade name, trademark, manufacturer, or otherwise does not necessarily constitute or imply its endorsement, recommendation, or favoring by the United States Government or any agency thereof. The views and opinions of authors expressed herein do not necessarily state or reflect those of the United States Government or any agency thereof.

DISCLAIMER

Portions of this document may be illegible in electronic image products. Images are produced from the best available original document.

DISCLAIMER

"This book was prepared as an account of work sponsored by an agency of the United States Government. Neither the United States Government nor any agency thereof, nor any of their employees, makes any warranty, express or implied, or assumes any legal liability or responsibility for the accuracy, completeness, or usefulness of any information, apparatus, product, or process disclosed, or represents that its use would not infringe privately owned rights. Reference herein to any specific commercial product, process, or service by trade name, trademark, manufacturer, or otherwise, does not necessarily constitute or imply its endorsement, recommendation, or favoring by the United States Government or any agency thereof. The views and opinions of authors expressed herein do not necessarily state or reflect those of the United States Government or any agency thereof."

This report has been printed directly from copy supplied by the originating organization. Although the copy supplied may not in part or whole meet the standards for acceptable reproducible copy, it has been used for reproduction to expedite distribution and availability of the information being reported.

Available from the National Technical Information Service, U. S. Department of Commerce, Springfield, Virginia 22161.

Price: Paper Copy $7.00
Microfiche $3.50

LMSC-D-766341
Distribution Category UC-63e

CADMIUM SULFIDE/COPPER SULFIDE HETEROJUNCTION CELL RESEARCH

Final Report

For Period February 26, 1979 – May 31, 1980

W. W. Anderson

A. D. Jonath

LMSC-D766341 June 1980

Work Performed Under Contract XJ-9-8033-1

Lockheed Palo Alto Research Laboratory
LOCKHEED MISSILES & SPACE COMPANY, INC.
3251 Hanover Street, Palo Alto, CA 94304

DISTRIBUTION OF THIS DOCUMENT IS UNLIMITED

ABSTRACT

Several all-sputter-deposited Cu_2S/CdS cells have been prepared to date with $J_{SC} \approx 3$ mA/cm^2 under simulated AM 1 illumination. The best AM 1 conversion efficiency obtained is 0.6%. This is typical of sputtered CdS in Cu_2S/CdS cells investigated to date. The sputtered Cu_2S appears to be satisfactory for solar cell applications.

Present evidence indicates that the poor conversion efficiency is due to a low-junction electric field intensity on the CdS side of the heterojunction. A multilayer CdS structure has been developed which may allow the tailoring of the junction electric field intensity to a selected high value to obtain high-junction collection efficiency.

Hybrid process cells consisting of sputter-deposited CdS with conventional dry processed Cu_2S were also prepared. The best of these cells exhibited a short-circuit current density of 6.9 mA/cm^2 and a conversion efficiency of 1.18 %.

CONTENTS

Section		Page
	ABSTRACT	iii
	ILLUSTRATIONS	v
	TABLES	vii
1	INTRODUCTION	1-1
2	INDIVIDUAL LAYER CHARACTERIZATION	2-1
	2.1 Cu_2S Characterization	2-1
	2.2 Thin Film Integrity	2-10
	2.3 CdS Characterization	2-12
3	DEVICE-MATERIAL PARAMETER CHARACTERIZATION	3-1
	3.1 Spectral Response	3-1
	3.2 Junction Collection Efficiency	3-7
	3.3 Hybrid Process Cells	3-15
	3.4 Cells from Modified Sputter Deposition System	3-20
4	CONCLUSION AND RECOMMENDATIONS	4-1
5	REFERENCES	5-1

ILLUSTRATIONS

Figure		Page
1	CdS/Cu_2S Solar Cell 653 Characteristics	1-2
2	Copper Nodule or Cone Growth in Cu_2S Deposited on CdS	2-3
3	SEM Cross Section of $Cu_2S/CdS/CdS{:}In$ Solar Cell Structure	2-4
4	Phase Diagram of the Cu-S System in the Range $1.70 \leq x \leq 2.00$ After Roseboom (Ref. 16)	2-6
5	Phase Diagram of the Cu-S System in the Range $1.70 \leq x \leq 2.00$ After Cook (Ref. 17)	2-7
6	DTA Scan of Reactively Sputtered Cu_xS	2-9
7	DTA Curves of Cu_xS in the Range $1.985 \leq x \leq 2.00$ After Guastavino (Ref. 15)	2-11
8	Individual Au Grid Line Characteristics for Cell No. 653	2-13
9	Individual Au Grid Line Characteristics for $Cu_2S/CdS/CdS{:}In$ Cells With High Resistivity Cu_2S	2-14
10	Resistivity Versus Substrate Temperature for Reactively Sputtered CdS Coatings	2-18
11	Resistivity of Reactively Sputtered CdS Versus Indium Content. Data from Ref. 19	2-19
12	Dependence of CdS Deposition Rate on H_2S Injection Rate and Substrate Temperature During Cylindrical Magnetron Reactive Sputtering. From Ref. 1	2-23
13	Resistivity Versus H_2S Injection Rate for Reactively Sputtered CdS Coatings	2-24
14	Spectral Reflectivity of Successive Layers of $Cu_2S/CdS/Nb$ Solar Cell Structure	3-2
15	Calculated Reflectivity of $Cu_2S/CdS/Nb$ Solar Cell Structure and of Cu_2S/CdS Structure	3-3
16	Maximum Short Circuit Current Obtainable From Cu_2S Layer With Back Surface Reflectivity and Minority Carrier Lifetime as Parameters	3-5
17	Spectral Response of All Sputter Deposited CdS/Cu_2S Cell No. 824	3-6

ILLUSTRATIONS (Cont.)

Figure		Page
18	Collected Photocurrent Squared Versus Device Voltage Under AM 1 Illumination for Two Cells	3-9
19	General Configuration of Multilayer CdS Sputter-Deposited Solar Cell	3-10
20	Capacitance-Voltage and Corresponding Ionized Impurity Concentration Versus Depth for Cu_2S/CdS/CdS:In Solar Cell Structure	3-11
21	I-V Characteristic of Cell No. 914 Which Shows Linear I-V Relation for $V < -0.1$	3-13
22	Development of Dark and AM 1 I-V Characteristic With Annealing at 190 C in H_2. Cell No. 824	3-14
23	Current-Voltage Characteristics of Cu_2S/CdS Cells With CdS Deposited by Two Different Processes	3-16
24	Volt-Ampere Characteristic of Hybrid Process Cell 967 in the Dark and Under AM 1 Illumination	3-19
25	Multicathode Magnetron Reactive Sputtering System Schematic for Sequential Deposition of Multilayer Films	3-21
26	Schematic Representation of Dependence of Resistivity on H_2S Injection Rate for Coatings Deposited Onto CdS	3-24
27	Schematic Diagram of Modified Multisource Deposition Apparatus	3-26
28	Single Grid Dark and AM 1 I-V Characteristics of As-Deposited Cells Prepared in Modified Deposition System	3-27

TABLES

Table		Page
1	Comparison of Device Characteristic Obtained to Computed Optimum (Ref. 1)	1-3
2	Short Circuit Current	1-3
3	DTA Summary	2-8
4	Cu_2S/CdS Cell Deposition Processes and Efficiencies Obtained	2-15
5	Thermodynamic Relations and Constants for CdS	2-21
6	Depletion Layer Widths	3-15
7	Cells With Cu_2S Applied by Institute of Energy Conversion	3-18
8	Heat Treatment of Hybrid Process CdS/Cu_2S Solar Cells	3-19

Section 1
INTRODUCTION

The program objective is to investigate and evaluate the application of cylindrical-post-magnetron reactive sputtering to the production of solar-cell quality thin films of CdS/Cu_2S for large-scale terrestrial photovoltaic energy conversion.

All sputter-deposited CdS/Cu_2S solar cell structures have been prepared. Deposition parameters are sufficiently well understood and controlled so that reproducible thin film material and device properties can be obtained from run to run. The I-V characteristic of the best cell prepared to date is shown in Fig. 1. In Table 1 the salient performance characteristics are compared with the optimum computed performance for this device. Computations are from Ref. 1 with V_{oc} for pure CdS and $L_n = 0.1\,\mu m$. It is obvious that the major deficit of the present device is in the short-circuit current. The fill factor is the second most serious problem.

Several cells have been prepared to date with $J_{sc} \approx 3$ mA/cm^2 under simulated AM 1 illumination as listed in Table 2. Cells 653 and 654 were prepared by cyclically sputtering Cd in H_2S/Ar and in pure Ar. Cells 824, 825, 917, and 920 were prepared by depositing 0.5 μm of undoped CdS onto 4 to 7 μm of CdS:In. Both sets of cells had wide depletion layers after heat treatment, even under AM 1 illumination, $W(AM1, V = 0) \approx 2\,\mu m$. Using Rothwarf's theory of field-aided collection across the heterojunction interface (Ref. 2), we find the poor short-circuit current to be primarily due to the low collection field in the CdS. Other current loss mechanisms such as grid shadowing and surface reflectance have been quantified and found to be small compared to the interface recombination.

The low fill factor may also be shown to depend on the interface recombination process in the cells. The open circuit voltage will increase with improved short circuit current. However, there is an additional voltage drop across the present junctions which has the characteristics of a TFL space charge limited current flow (Ref. 3).

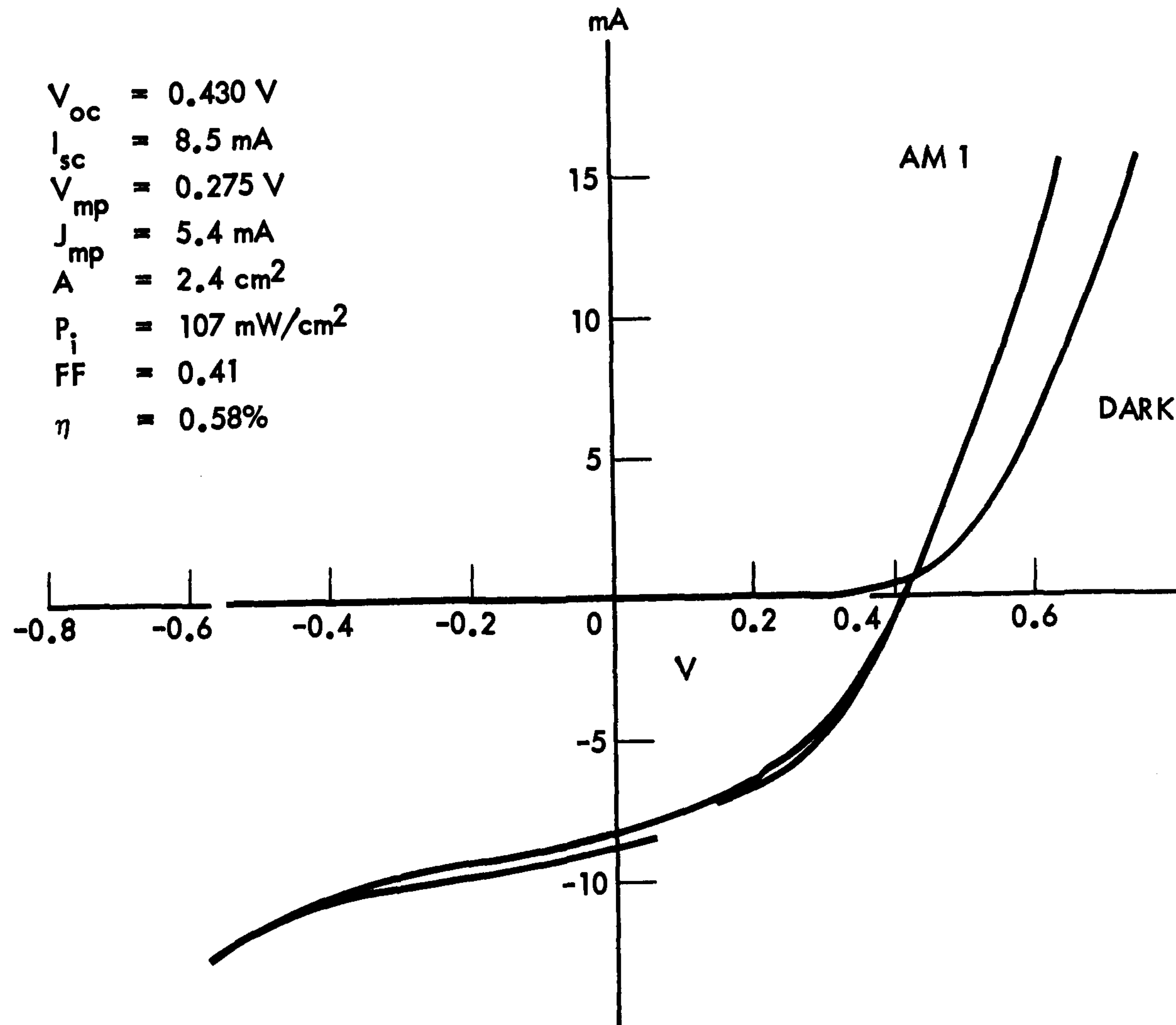

Fig. 1 CdS/Cu_2S Solar Cell 653 Characteristics

Table 1

COMPARISON OF DEVICE CHARACTERISTICS OBTAINED TO COMPUTED OPTIMUM (REF. 1)

Parameter	Measured	Optimum	Ratio
J_{SC} (mA/cm^2)	3.4	15.5	0.22
FF	0.41	0.8	0.51
V_{oc} (V)	0.43	0.54	0.80
η (%)	0.58	6.5	0.09

Table 2

SHORT CIRCUIT CURRENT

Cell No.	Isc (mA)	A (cm^2)	Jsc (mA/cm^2)
653	8.5	2.4	3.5
654	10	3.75	2.7
824	8.0	2.18	3.7
825	5.2	2.43	2.14
917	8.8	3.58	2.46
920	10	3.76	2.66

Hybrid process cells consisting of sputter-deposited CdS with conventional processed Cu_2S were also prepared. The best of these cells exhibited a short-circuit current density of 6.9 mA/cm^2 and a conversion efficiency of 1.18%. The reverse I-V characteristic of the hybrid process cells did not appear to exhibit the voltage-dependent current collection efficiency of the all sputter-deposited CdS/Cu_2S solar cell structures.

Section 2
INDIVIDUAL LAYER CHARACTERIZATION

2.1 Cu_2S CHARACTERIZATION

It has been generally accepted that chalcocite is the desired Cu_xS phase for solar cell applications (Refs. 4, 5). Refined analysis of the Cu_2S/CdS cell suggests an optimum departure of Cu_xS from stoichiometry ($x = 2$) to $x = 1.9995$ (Ref. 6) which is within the chalcocite phase existence region (Ref. 7). Early in this program we established the phase/H_2S pressure/substrate temperature relationship for Cu_xS deposited onto glass substrates (Ref. 8). Three important results were derived from this work:

- A "resistivity gap" exists between the chalcocite phase and the lower Cu content phases. High room temperature resistivity ($\rho \sim 10$ to 10^2 Ω-cm) is adequate to identify the predominence of the chalcocite phase
- Excess Cu precipitates out in the form of Cu nodules or cones. The presence of Cu nodules is sufficient but not necessary to identify a film as predominantly chalcocite
- The optical absorption characteristics of Cu_xS films are accurately described by the empirical relations determined from single crystal studies (Refs. 8, 9, 10)

This early work was partially repeated to verify that similar deposition parameter/ Cu_xS phase relations existed when Cu_xS was sputtered onto a CdS film. It was found that similar relations do exist and that chalcocite is readily obtained. New information on the importance of chamber wall effects specific to the Cu_2S deposition process was obtained from this second study (Refs. 11, 12). Thick films of Cu_xS were subjected to differential thermal analysis (DTA) in order to determine if the Cu/S ratio can be found by comparison with single crystal DTA data.

A significant finding of the Cu_2S deposition study was:

- Cu cones do not result in excessive cell shunt conductance

An early result of studies on Clevite cells showed that Cu nodule growth down grain boundaries resulted in cell degradation (Ref. 5). The growth characteristic of Cu nodules in sputter-deposited Cu_2S is up from the CdS top surface through the Cu_2S film as shown in the SEM photo of Fig. 2a. The depth of the hole left where the Cu cones have "fallen out" is 0.15 μm, i.e., the thickness of the Cu_2S layer only. Some surface texture results when a thick CdS film is grown as shown in Fig. 2b, but the Cu cone formation is essentially the same as on a smooth surface. Figure 2b is the top surface of Cell 803. There was no evidence of shunting conductance due to the high density of Cu cones. The very dense CdS film produced by sputtering precludes Cu nodule growth down to the metallic substrate. (See Fig. 3.)

A definite deleterious effect of Cu cone formation is reduction of a portion of the active surface of the cell, resulting in a reduced short-circuit current. Cell 824 had a fractional area coverage of only 0.36% while Cell 920 had a fractional area coverage of 19.5% due to Cu cones. Earlier experiments on Cu_2S over glass substrates showed a constant "effective" absorption constant for $\lambda > 1.1$ μm which was determined by the fractional area covered by Cu cones (Fig. 13 of Ref. 8).

A possible deleterious effect is reduction of open circuit voltage. From Fig. 2a we see that the Cu may physically contact the CdS surface. Cu forms a Schottky barrier to CdS with $\phi_B = 0.35$ V on an atomically clean CdS surface (Refs. 13, 14), but with $\phi_B = 0.7$ V on a slightly oxidized surface (Ref. 14). For $\phi_B = 0.35$ V, a reduced open circuit voltage may result due to forward biasing of the Cu/CdS Schottky barrier regions.

The Cu cone density on Cells 824 and 825 was too insignificant to affect either the short-circuit current or the open-circuit voltage. The recent Cu_2S deposition study has shown that, with a heated CdS substrate ($T_s \approx 150$ C),

- Increasing H_2S partial pressure during deposition reduces the Cu cone density (Ref. 12).

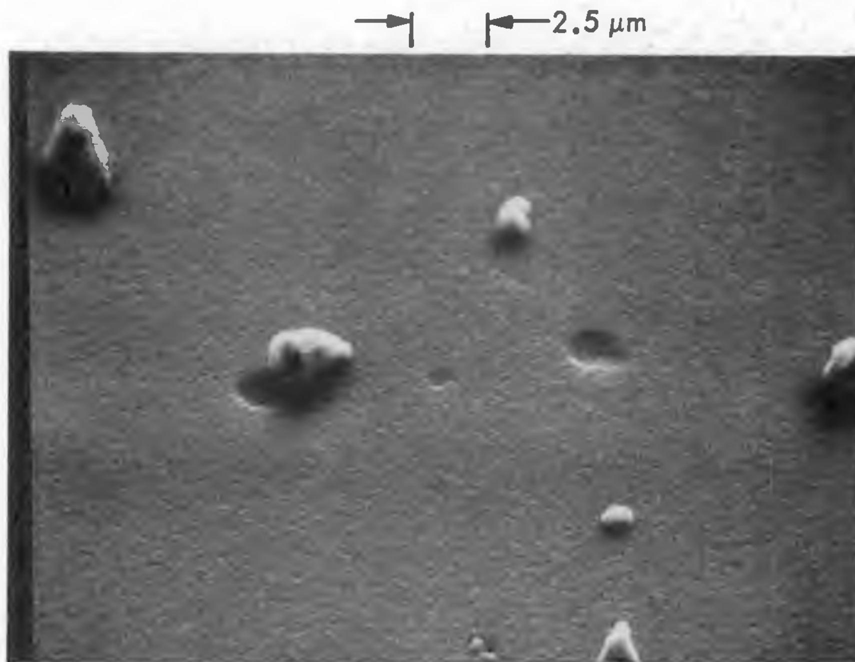

a. Cu Cone formation in Cu_2S grown over 0.5-μm thick CdS

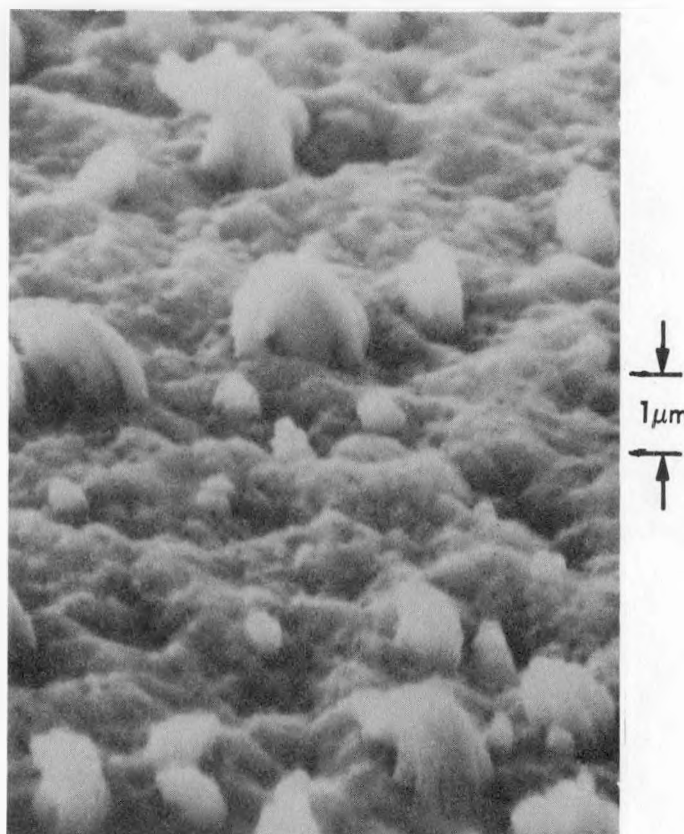

b. Cu Cone formation in Cu_2S grown over 7-μm thick CdS

Fig. 2 Copper Nodule or Cone Growth in Cu_2S Deposited on CdS

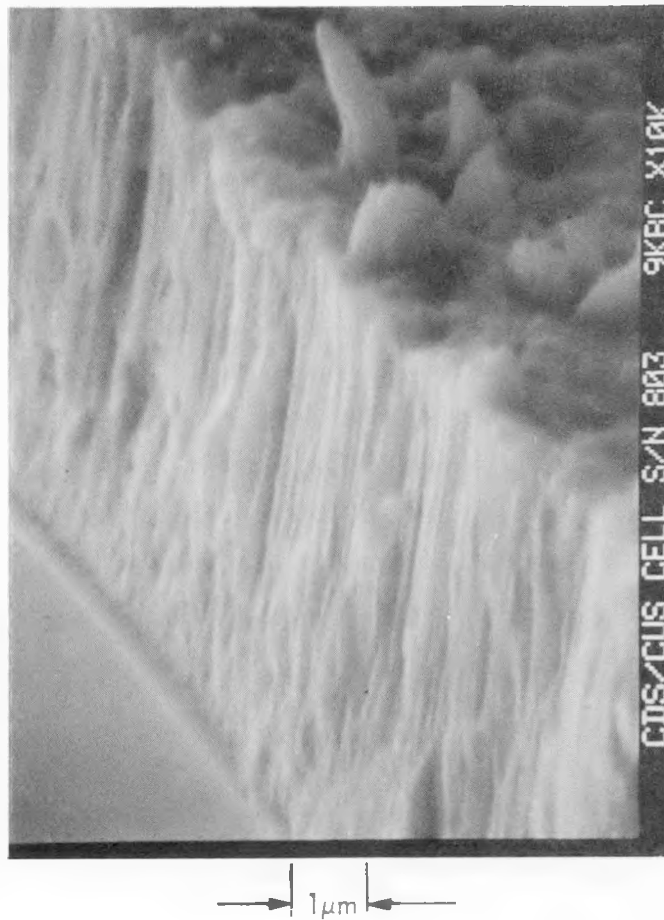

Fig. 3 SEM Cross Section of Cu_2S/CdS/CdS:In Solar Cell Structure

The initial photo-electronic interaction in the Cu_2S/CdS cell takes place in the Cu_2S layer of the cell. Optical absorption and cell short-circuit current spectral response measurements indicate that sputter-deposited Cu_2S has optical characteristics close to conventional topotaxially grown Cu_2S. Cell photocurrent spectral response measurements also indicate minority carrier (electron) diffusion lengths comparable to those of conventional cells (L_n ~0.1 to 0.3 μm). Analysis indicates that present device limitation occurs at the Cu_2S/CdS interface. Therefore, the present status of sputter-deposited Cu_2S may be considered acceptable while the CdS and interface are investigated. When satisfactory junction collection efficiency is obtained, the Cu_2S study can be resumed to maximize V_{oc}, minimize series resistance, maximize minority carrier diffusion length, and minimize surface recombination velocity.

Thick films of Cu_xS deposited on Corning 7059 glass at a substrate temperature of 150 C were subjected first to x-ray analysis (XRD) and then removed for differential thermal analysis (DTA). The predominant lines seen in the XRD correspond to orthorhombic chalcocite. Lines of secondary intensity corresponding to djurleite and to copper are present and there are also additional lines of low intensity.

The samples were subjected to DTA in order to determine if the Cu/S ratio can be found by comparison with single crystal DTA measurements made by Guastavino (Ref. 15) and with reference to the Cu-S system phase diagrams of Roseboom (Ref. 16), Fig. 4, and Cook (Ref. 17), Fig. 5. Our DTA measurements were made on a Mettler TA2000B Thermal Analysis System. Care was taken throughout the measurement to exclude oxygen by using a dry nitrogen atmosphere. No Cu-O phases were detected; Cu-N phases are only formed at temperatures significantly higher than the range of the experiment.

Approximately 5 mg of Cu_xS sample is placed in the sample chamber and the differential temperature between it and a reference chamber is monitored. Endothermic or exothermic phase changes appear as negative or positive peaks,

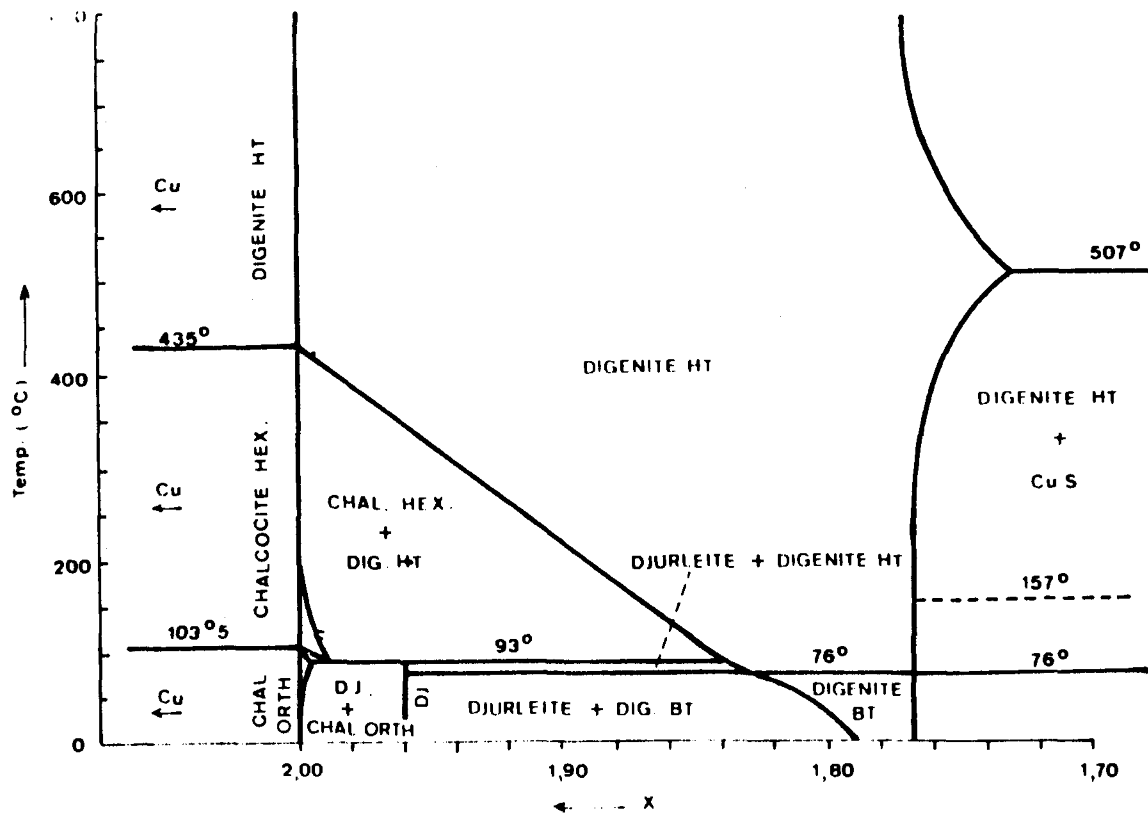

Fig. 4 Phase Diagram of the Cu-S System in the Range $1.70<x<2.00$ After Roseboom (Ref. 16).

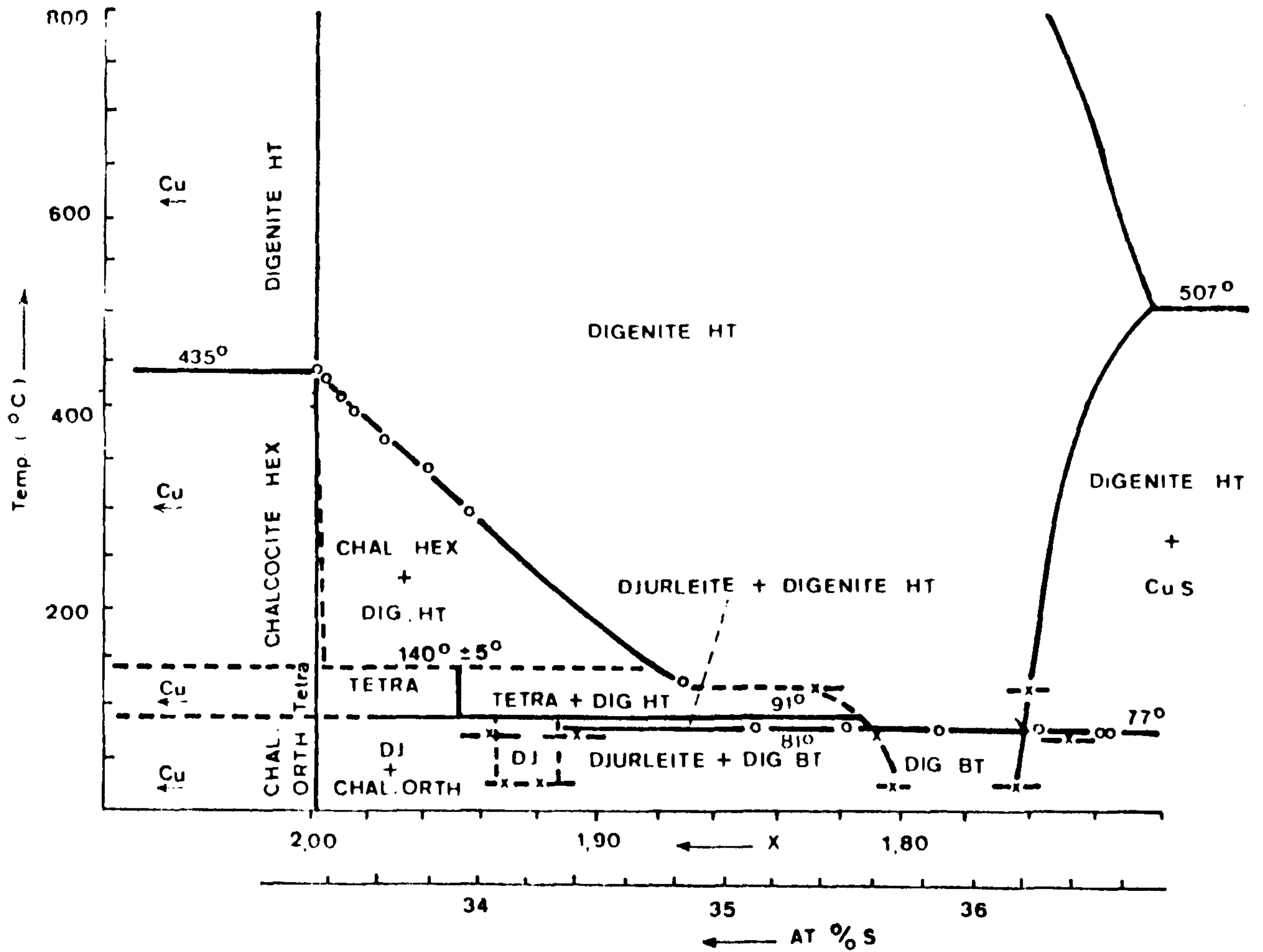

Fig. 5 Phase Diagram of the Cu-S System in the Range 1.70<x<2.00 After Cook (Ref. 17)

respectively, on a thermogram shown in Fig. 6. The endotherm at $104.6 < T < 106C$ on the heating curve represents a phase change from orthorhombic chalcocite to hexagonal chalcocite and corresponds to structure in the electrical resistivity thermograms reported earlier (Ref. 9). The exotherm corresponding to the reverse change occurs at $82 > T > 72.7C$. This hysteresis, also observed in both electrical resistivity and single crystal DTA measurements, is caused by a metastable phase whose temperature existance region is determined by the cooling rate.

The data for several scans are summarized in Table 3.

Table 3

DTA SUMMARY

Scan No.	dT/dt (C/min)	T_t^* (C)	T_{max} (C)	ΔH_t (J/g)
2	2	103.8	105.6	-
3	5	103.6	106.9	-
4	-5	75.2	72.7	-
5	5	103.7	106.0	+12.0
6	-5	75.2	72.8	-10.1
7	2	104.0	105.6	+11.2
8	2	104.1	105.6	+12.3
9	-2	75.9	73.8	-14.9
10	-5	75.6	72.9	-10.7
13	2	103.3	104.6	+12.0
2-1	1	104.8	106	-
2-2	-1	85.0	82.0	-

* T_t = transition temperature at 10% peak height.

The average value of the heat of reaction is $[\Delta H_t] = 11.9$ J/g ± 1.5 ≈ 0.45 kcal/mole. This was calculated assuming the entire sample weight to be chalcocite. For the Cu/S ratio inferred from these DTA data, as discussed below, this assumption is valid.

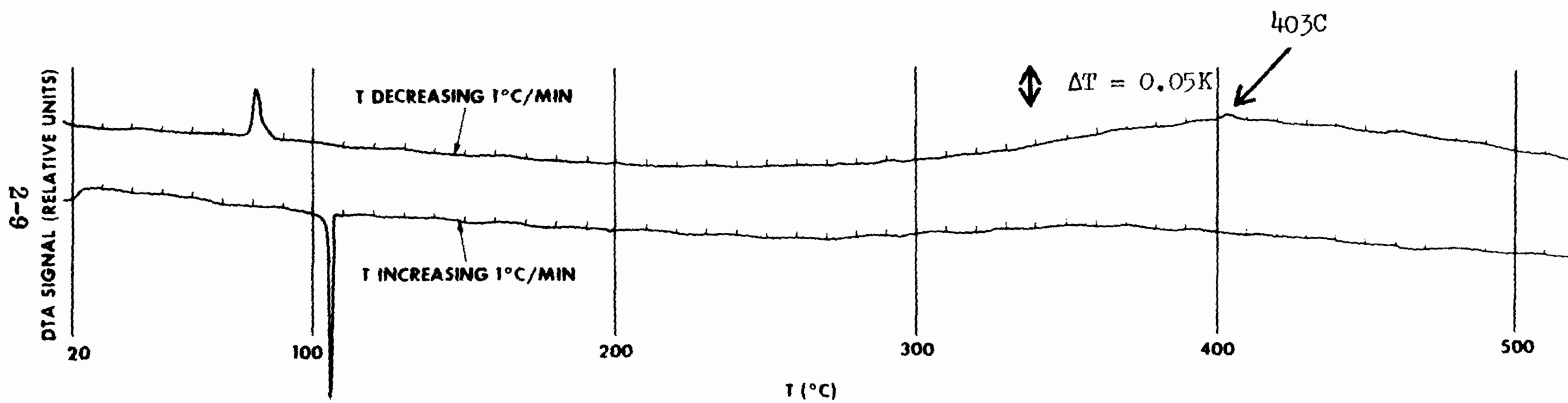

Fig. 6 DTA Scan of Reactively Sputtered Cu_xS

The scans shown in Fig. 6 are No. 2-1 and No. 2-2 for which a second sample from the same deposition run was prepared for high temperature DTA, up to 520C. The purpose was to explore the 435 C temperature region (see Figs. 4 and 5) for evidence of the hexagonal chalcocite to high-temperature digenite phase transformation. Although no evidence of this phase change is seen on the heating scan, a small but distinct "bump" is observed at $406 > T > 400C$ on the cooling curve. We attribute this exotherm to the 435C phase change. It is probably shifted down in temperature by 20 to 30C due to hysteresis effects similar to those observed separating the low-temperature endotherm and exotherm. That the peak does not show on heating is discussed later.

We next compare these results to the single crystal DTA scans of Ref. 15 which are shown in Fig. 7. These scans depict endotherms only; the sign of the ordinate is arbitrary. The left (low-temperature) scan shows a doublet up to $x = 1.995$. The low temperature part of the doublet ($T \approx 93C$) is caused by significant presence of djurleite below this composition. Our thick-film sample shows no doublet.

The right scan in Fig. 7 shows the appearance of the high-temperature endotherm at $1.992<x<1.995$. Assuming the exotherm peak height to be less than that of the endotherm, one might also infer $x \approx 1.995$ from this result.

The conclusion we draw from these results is that the Cu/S ratio in reactively sputtered Cu_xS is $1.995^{+0.002}_{-0.001}$. That the high-temperature endotherm does not appear on heating might indicate that there already exists at the deposition temperature a small amount of metastable HT digenite and the very small additional amount formed upon heating is not noticed. But upon cooling, at the slowest rate, all this HT digenite changes to hexagonal chalcocite and the weak exotherm appears. It would be interesting to perform the XRD on a hot stage and to repeat the full-temperature DTA scan to see if the endotherm now appears in this sample.

2.2 THIN FILM INTEGRITY

Cu_2S/CdS composite films are deposited over 5 cm^2 of a 6.5 cm^2 Nb-coated glass substrate. An array of 31 Au fine-line grids is then deposited over 4.1 cm^2 of the

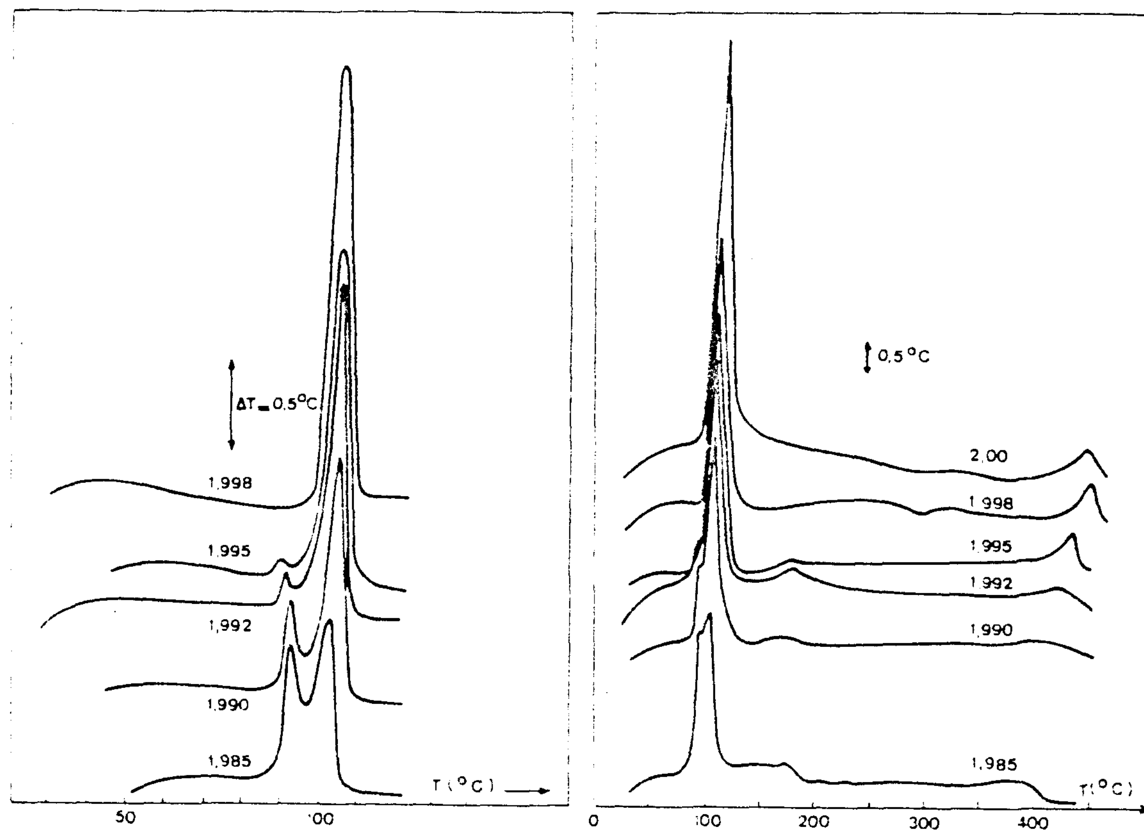

Fig. 7 DTA Curves of Cu_xS in the Range $1.985 < x < 2.00$. After Guastavino (Ref. 15).

Cu_2S/CdS area. (Note that all the cell areas listed in Table 2 are less than total gridded area. The most common reason for reduced active area was associated with excessive Au grid width due to lifting of the grid deposition mask. Opaque Au areas were simply removed by scribing the cell surface.)

Individual Au grid lines are probed for evaluation of device characteristics before an interconnect bus bar is deposited. When low leakage diode characteristics are observed, the Cu_2S resistivity may be obtained from the resistance measured between two adjacent Au grid lines.

Three distinct cases are typically observed from an individual Au grid line evaluation:

- Isolated poor diode characteristics that strongly influence adjacent Au grid line diode characteristics; this immediately indicates a low resistivity Cu_2S phase (Fig. 8a)
- Isolated poor diode characteristics with no discernible effect on adjacent Au grid line diode characteristics; this immediately indicates a high resistivity (chalcocite) Cu_2S phase (Fig. 9a)
- All Au grid line diode characteristics similar (Fig. 9b). This is now a typical observation as a result of improved substrate cleaning and handling procedures

Localized areas of a device may be isolated by scribing the film surface. This was done on the device shown in Fig. 8. The remaining area (grids 12 through 31 interconnected) gave the large area cell characteristic presented in Fig. 1. Similarly, small areas of a device may be isolated for detailed I-V and/or C-V measurements.

2.3 CdS CHARACTERIZATION

A representative review of the results of sputter deposition as applied to the Cu_2S/CdS cell is given in Table 4. With allowance made for the relative effort expended to date on the various process combinations given in Table 4, it is evident that the main problem is with material properties of the sputtered CdS layer.

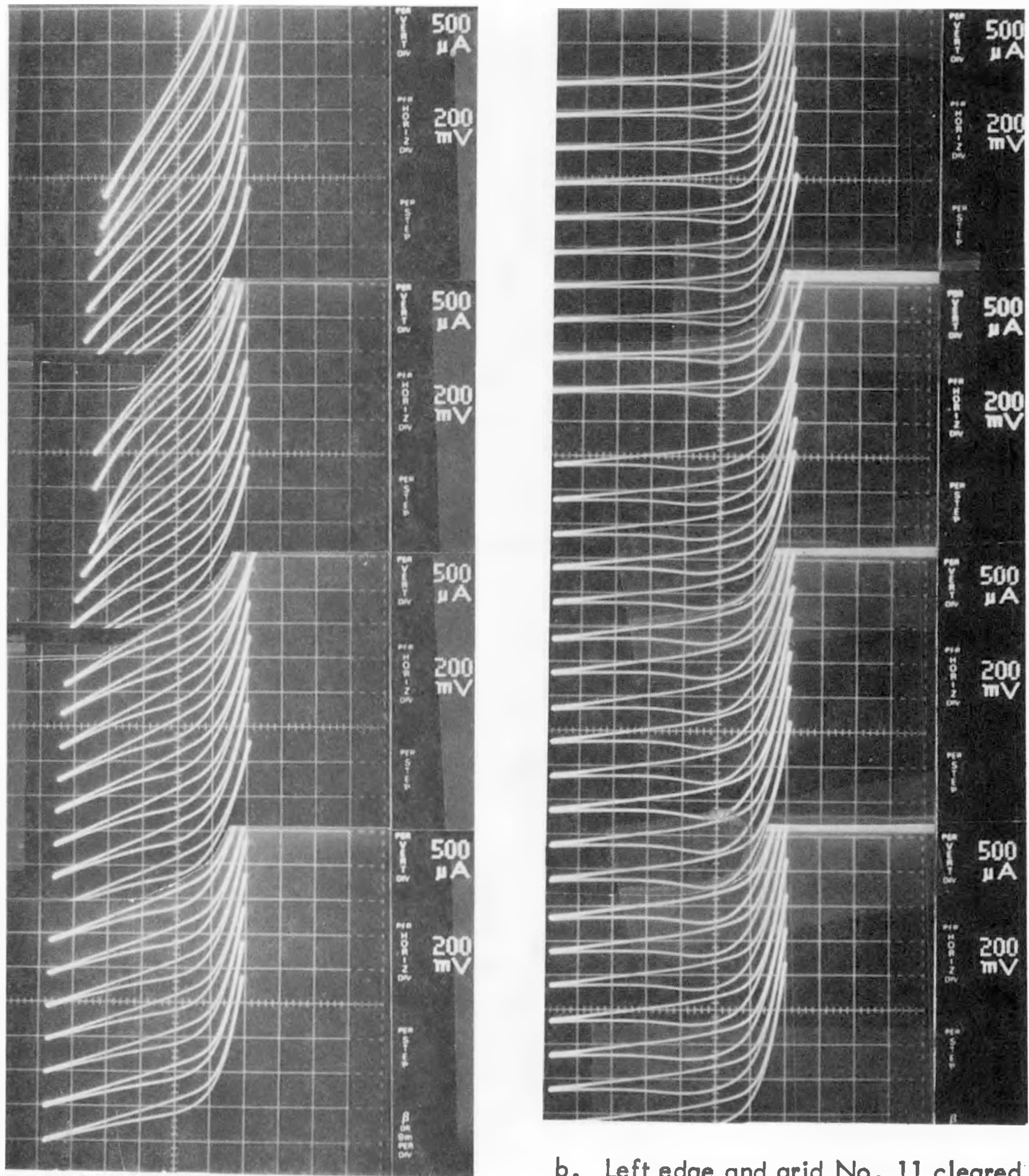

b. Left edge and grid No. 11 cleared

a. As deposited.

Fig. 8 Individual Au Grid Line Characteristics for Cell No. 653

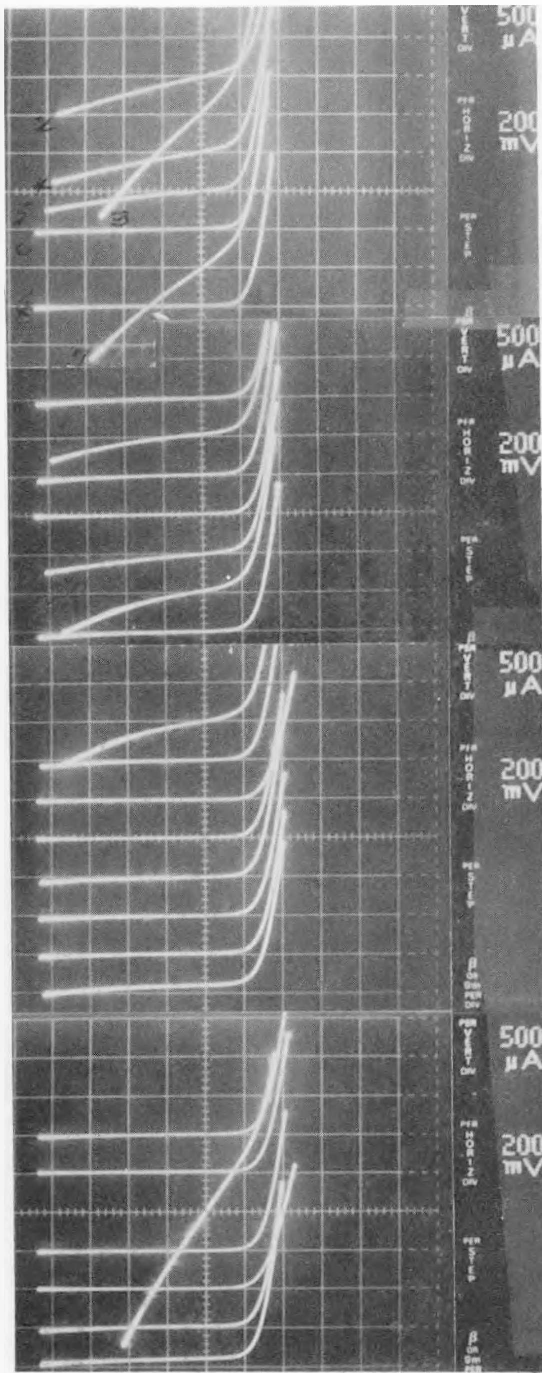

a. Cell No. 804

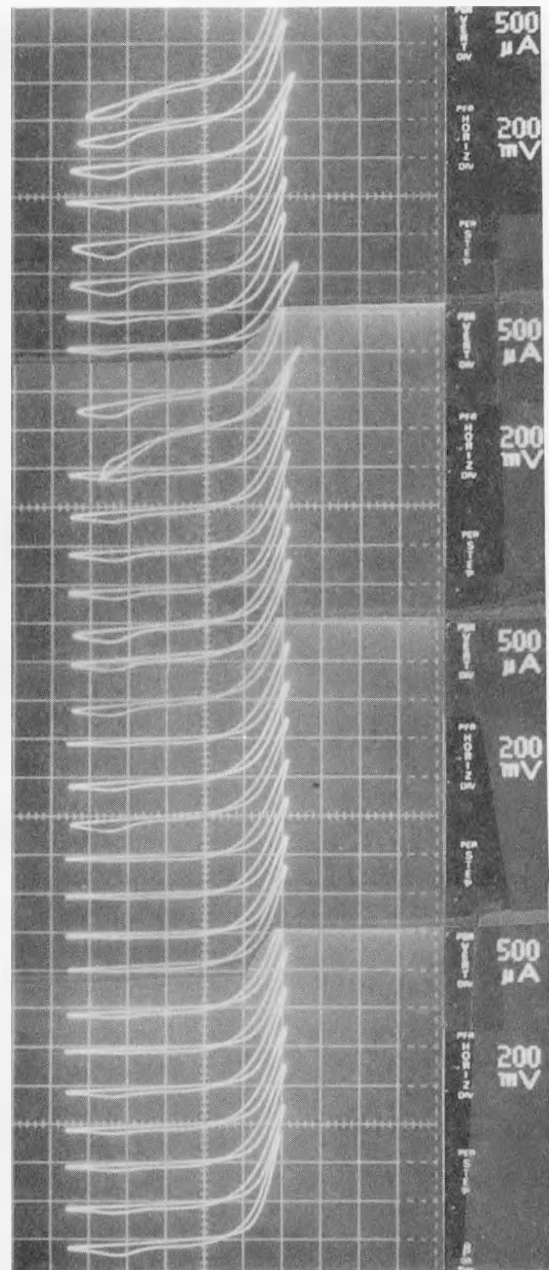

b. Cell No. 807

Fig. 9 Individual Au Grid Line Characteristics for Cu_2S/CdS/CdS:In Cells With High Resistivity Cu_2S

Table 4

Cu_2S/CdS CELL DEPOSITION PROCESSES AND EFFICIENCIES OBTAINED

		Cu_2S	
		Conventional (a)	Sputtered (b)
Cds	Conventional	IEC [1] ≈9% Westinghouse [2] ≈6% U. of Stuttgart [3] ≈7%	LLL [4] ≈4% Annamalai [5] <2%
	Sputtered (b)	Leybold-Heraeus [6] ≈.8% Efremenkova, et al. [7] <1% R. Hill [8] <1% LMSC/Telic/IEC [10] ≈1.2%	Leybold-Heraeus [6] ≈1% LMSC/Telic [10] ≈0.6% LLL [9] <1%

(a) Includes both wet dip and dry barrier processes

(b) Includes inert gas and reactive sputtering both with and without magnetic plasma confinement

[1] J. D. Meakin et al., Institute of Energy Conversion, Final Report on Contract EG-77-C-03-1536 (May, 1979)

[2] J. R. Szedon et al., Westinghouse R&D Center, Final Report on Contract DE-AC03-77 ET20429 (July, 1979)

[3] W. Arnolt et al., 2nd E. C. Photovoltaic Solar Energy Conference, ed. by R. VanOverstraeten and W. Palz, D. Reidel Publ. Co., Dordrecht (1979), pp 826-842

[4] G. A. Armantrout, Lawrence Livermore Laboratory, Tech. Status Report 1/1/77-6/30/78 on Contract W-7405-Eng-48 (Jan 1979)

[5] N. K. Annamalai, 12th IEEE Photovoltaic Specialists Conference, 1976, pp 547-548

[6] W. Muller et al., Thin Solid Films 59, 327 (1979)

[7] V. M. Efremenkova et al., Izv. Acad. Nauk. SSSR, Ser. Fiz. 32, 1242 (1968)

[8] R. Hill, Newcastle upon Tyne Polytechnic, private communication (Jan 1980)

[9] G. A. Armantrout and L. D. Partain, Contractors Indepth Review Meeting, SERI (Feb 1979)

[10] This work

Early in this study of CdS and $Cd_{0.9}Zn_{0.1}S$ deposition by reactive sputtering, it became evident that some features of the sputter deposition process were qualitatively different from the high rate, single source, vacuum evaporation process. The bottom line result is that conductivity control by a stoichiometric excess of Cd is difficult by the sputtering process. Theoretical considerations relevant to sputter deposition of a compound, both constituents of which are separately quite volatile at the substrate temperatures of interest, were given in Ref. 1.

The slow film deposition rate via the sputtering process ($R \approx 1 - 2\,\mu m/h$ at substrate temperatures $T_s \sim 250 - 300$ C) allows the growing film to more nearly approach its thermal equilibrium state. Vacuum evaporation deposition is normally carried out at a much higher rate, $R \approx 1\text{–}2\,\mu m/min$ (Ref. 18) and with an excess of Cd in the vapor stream (Ref. 5). An artificially high Cd flux can be introduced in the sputtered vapor stream by reducing the H_2S partial pressure cyclically or in the steady state. By cyclically sputtering Cd in Ar/H_2S and Ar, CdS films with $\rho = 10^3\ \Omega$-cm were obtained. (This deposition process was used to prepare Cells 653 and 654. See Fig. 1 and Tables 1 and 2.)

An alternative to deviation from stoichiometry resistivity control is impurity doping. Considerable experience with In as a dopant is available from the early Clevite work (Ref. 5). Cells with 6% conversion efficiency were produced. There is a high degree of dopant distribution control available in the reactive sputter deposition process. Of particular interest and importance is the ability to change dopant and/or alloy composition during deposition by switching cathodes. The SEM cross section shown in Fig. 3 is a composite of 0.5-μm undoped CdS on top of 7.0 μm of 1.0% In-doped CdS. Note that there is no discernible discontinuity in the columnar grain structure when the deposition cathodes were switched. The electrical characteristics of this composite CdS layer are described in section 3.2 in relation to device characteristics.

Resistivity Control by Doping

Figure 10 shows the resistivity versus substrate temperature for CdS coatings deposited by reactive sputtering from undoped Cd targets and from targets with 0.1 and with 1 at. % In. The coatings were approximately 150-nm thick and were deposited onto glass substrates having pre-deposited Nb diagnostic electrodes that permitted resistivity and electron mobility measurements in the plane of the film The mobilities of the 1 at. % In coatings were measured and found to be about 10 $cm^2/V\text{-}s$. The carrier concentrations were about 7×10^{18} cm^{-3}, indicating that about 3.5% of the In atoms contributed electrons to the conduction band (Ref. 11).

Figure 11 shows the resistivity and electron mobility versus indium content for reactively sputtered CdS coatings which were doped by codeposition from a separate In source during the previous program (Ref. 1). The In content was determined from microprobe measurements. The figure is plotted from data given in Fig. 13 of Ref. 19. The resistivity of the coatings deposited using the doped cathodes (Fig. 10) is seen to be consistent with data obtained by Cd and In codeposition (Fig. 11).

Role of Cadmium Vacancies

In CdS crystals, S vacancies and Cd interstitials form donor levels, while Cd vacancies form acceptor levels. The donor levels are relatively close to the conduction band (0.05 and 0.2 eV). By contrast, the Cd vacancy levels are much farther from the valence band. Consequently, CdS tends to be an n-type semiconductor.

Indium doping atoms on Cd sites form donors in the CdS crystal. The In_{Cd} donor level is close to the conduction band, so that ionization is always complete (Ref. 20). However, if the energy which can be recovered by transferring an electron from the In donor to the Cd vacancy acceptor level is larger than the energy required for Cd vacancy formation, then it is energetically favorable for the crystal to form Cd vacancies which compensate the incorporated In donors (Ref. 21). The probability for self-compensation becomes high in large-bandgap materials (Ref. 21) such as the highly ionic II-VI compound semiconductors (Ref. 22).

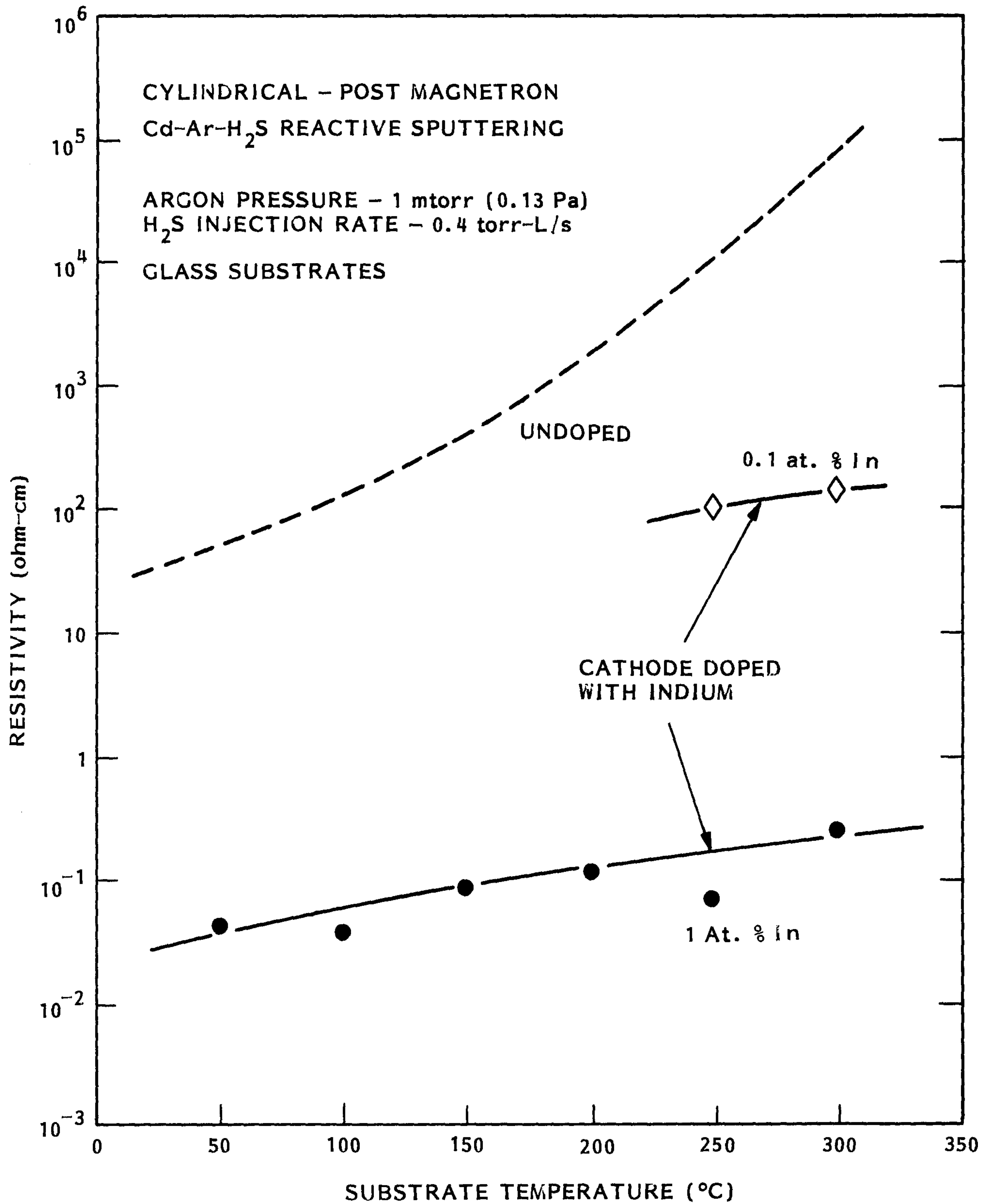

Fig. 10 Resistivity Versus Substrate Temperature for Reactively Sputtered CdS Coatings

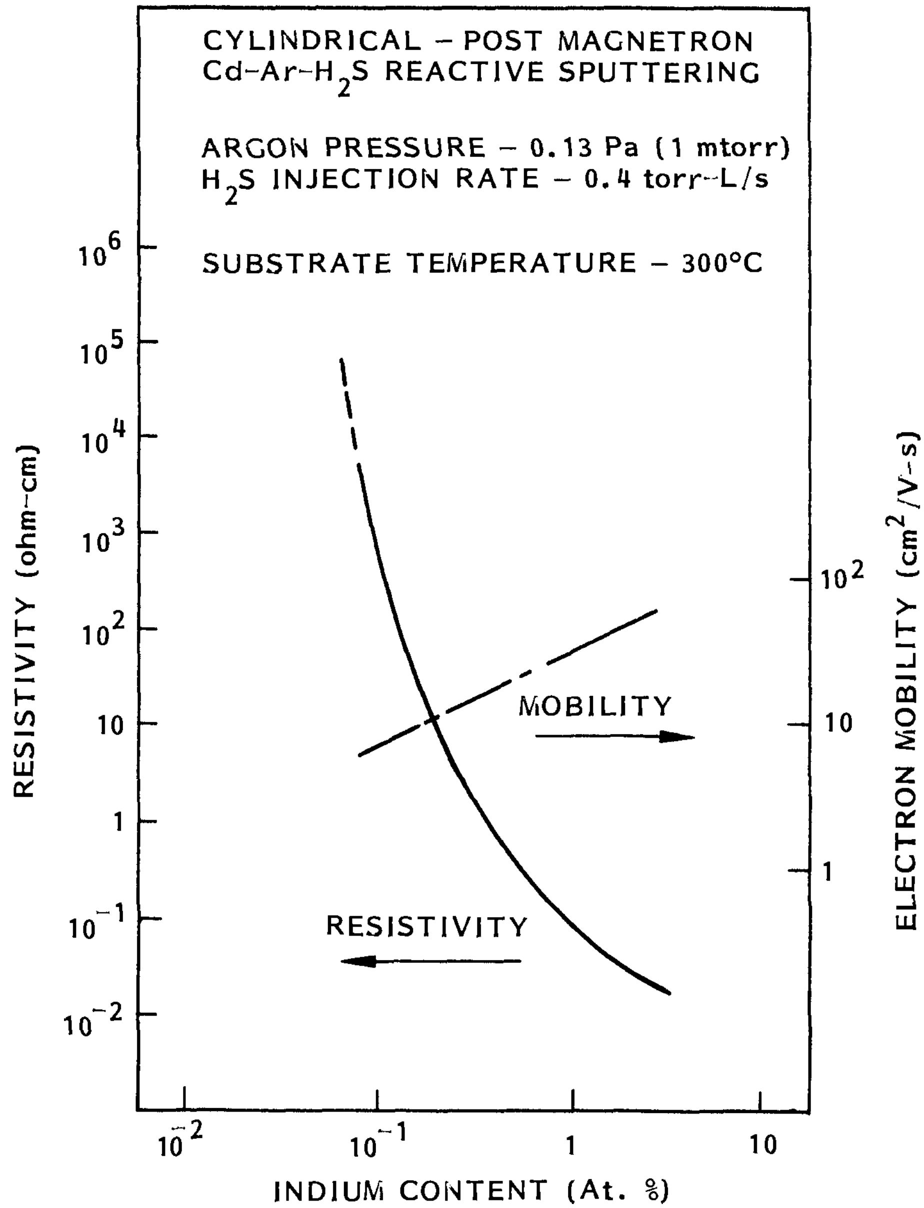

Fig. 11 Resistivity of Reactively Sputtered CdS Versus Indium Content. Data from Ref. 19.

Thus, in order to obtain a high conductivity in both undoped and doped CdS, it is necessary that the Cd vacancy level be minimized (Ref. 23). Equilibrium calculations and experimental observations (Ref. 24) confirm that a high Cd vapor pressure over a CdS crystal minimizes Cd vacancy formation and enhances the effectiveness of In doping.

Equilibrium defect density calculations in CdS are based on the thermodynamic relations listed in Table 5. Defects are identified as Cd interstitials, Cd_i , or vacancies, V_{Cd} , although the microscopic identity of the electrically active native defect is ambiguous. Singly and doubly ionized doner-type defect densities are indicated by $[Cd_i^{\cdot}]$ and $[Cd_i^{\cdot\cdot}]$, respectively, while singly and doubly ionized acceptor-type defect densities are indicated by $[V_{Cd}^{\prime}]$ and $[V_{Cd}^{\prime\prime}]$ respectively. Neutral defect densities are $[Cd_i]$ and $[V_{Cd}]$. The numerical values given in Table 5 are from Nebauer (Ref. 25). The ionization energies of the defects associated with equilibrium constants K_2, K_3, K_5, K_6, and K_{eh} are from relatively low-temperature measurements and may not be valid at the deposition temperature used in reactively sputtering CdS ($T_s \approx 250C = 523$ K). However, these relations provide insight into the problem of conductivity control by doner doping and native defect density effects. At 250C, the dominating charge neutrality relation is $2[V_{Cd}^{\prime\prime}] = Nd$ for $6 \times 10^{-7} > p_{Cd} > 3.4 \times 10^{-27}$ atm (equivalent to $10^{14} > p_{S_2} > 3 \times 10^{-27}$ atm on the basis of K_{CdS} as given in Table 4). While the equilibrium constants listed in Table 5 are subject to considerable uncertainty, expecially the acceptor ionization energies used in K_2 and K_3, the conclusion that charge compensation occurs via the doubly charged acceptor defect remains valid for most reasonable acceptor ionization energies and all accessible partial pressures of Cd and S_2. It may be fortuitous but still worth noting that the Cd partial pressure corresponding to the transition to doner dopant controlled conductivity, $p_{Cd} \approx 6 \times 10^{-7}$ atm, corresponds to a Cd deposition rate of $2\,\mu m/min$. This is close to the deposition rate for evaporative deposition of CdS but an order of magnitude higher than the reactive sputter deposition rate used to date.

Table 5

THERMODYNAMIC RELATIONS AND CONSTANTS FOR CdS

Property or Relation		Value or Description
$p_{Cd}^2 p_{S_2} = K_{CdS}$ (atm.^{3})	=	$4 \times 10^{20} \exp\left(\frac{-6.75\text{eV}}{kT}\right)$
$[V_{Cd}] = K_1 p_{S_2}^{1/2}$	=	$\{1.29 \times 10^{15} \exp\left(\frac{-1.12\text{eV}}{kT}\right)\} p_{S_2}^{1/2}$
($[V_{Cd}]$ in cm^{-3}; p_{S_2} in atm.)		
$[V'_{Cd}]\,[V_{Cd}]^{-1}\,n^{-1} = K_2\ (cm^3)$	=	$2N_c^{-1} \exp\left(\frac{1.9\text{eV}}{kT}\right)$
$[V''_{Cd}]\,[V'_{Cd}]^{-1} n^{-1} = K_3\ (cm^3)$	=	$0.5N_c^{-1} \exp\left(\frac{1.3\text{eV}}{kT}\right)$
$[Cd_i]\,[V_{Cd}] = K_4 (cm^{-6})$	=	$4 \times 10^{44} \exp\left(\frac{-5.45\text{eV}}{kT}\right)$
$[Cd_i^{\cdot}]\,[Cd_i]^{-1} n = K_5\ (cm^{-3})$	=	$2N_C \exp\left(\frac{-0.05\text{eV}}{kT}\right)$
$[Cd_i^{\cdot\cdot}]\,[Cd_i^{\cdot}]^{-1} n = K_6\ (cm^{-3})$	=	$0.5\ N_C \exp\left(\frac{-0.20\text{eV}}{kT}\right)$
$pn = K_{eh}\ (cm^{-6})$	=	$N_C N_V \exp\left(\frac{-Eg}{kT}\right)$

Woodbury prepared In-doped CdS samples by diffusing In into the crystals (Ref. 24). Samples were prepared with In levels ranging from about 10^{17} cm^{-3} to very degenerate cases having In contents of about 10^{20} cm^{-3}. Carrier concentrations were much lower than the doping levels (e.g., doping level of 10^{20} cm^{-3} yielded carrier concentration of $8x10^{17}$ cm^{-3}), unless the samples were fired in Cd vapor for a few hours at a relatively high temperature (800 C). With this type of treatment, a 1:1 correspondence was obtained between the In content, as determined spectroscopically, and the room temperature carrier concentration, for carrier concentrations ranging from 10^{20} cm^{-3} down to the donor impurity level of about 10^{17} cm^{-3}.

Experimental evidence of the Cd vacancy effects described above have been seen in the reactively sputtered coatings. Figure 12 from our previous work (Ref. 1) shows the dependence of the deposition rate on the H_2S injection rate and substrate temperature for cylindrical magnetron reactive sputtering of Cd in H_2S. At high H_2S injection rates, point A Fig. 12, the deposition rate is limited by the available Cd flux. At low injection rates, point B Fig. 12, the sulfur flux is rate-limiting. The deposition rates decrease with increasing substrate temperature because of the reduced sticking coefficients. The coatings in Figs. 10 and 11 were deposited just to the left of the knee (point C) of the curve in Fig. 12; i.e., in the Cd-rich, S-deficient region where the Cd vacancy level might be expected to be reduced. Figure 13 shows the resistivity versus H_2S injection rate for doped and undoped CdS coatings deposited at a fixed substrate temperature of 250 C. The doping is seen to rapidly increase in effectiveness as the H_2S injection rate is reduced sufficiently to pass into the range (B in Fig. 12) where the H_2S flux and not the Cd flux is rate-limiting in the deposition process. Microprobe measurements for the 1 at. % In case confirmed that the high resistivity coatings deposited at large H_2S injection rates did indeed contain 1 at. % of In. The resistivity of the undoped material is also seen to be reduced by about an order of magnitude as the H_2S injection rate is decreased. Additional work is required to determine the reason for the apparent "lower limit" to the resistivities that were obtained under sulfur-deficient conditions using the undoped and 0.1 at. % In targets.

Pulsed H_2S injection also reduces the Cd vacancy level and therefore the resistivity of coatings deposited with an undoped cathode. This method successfully reduced

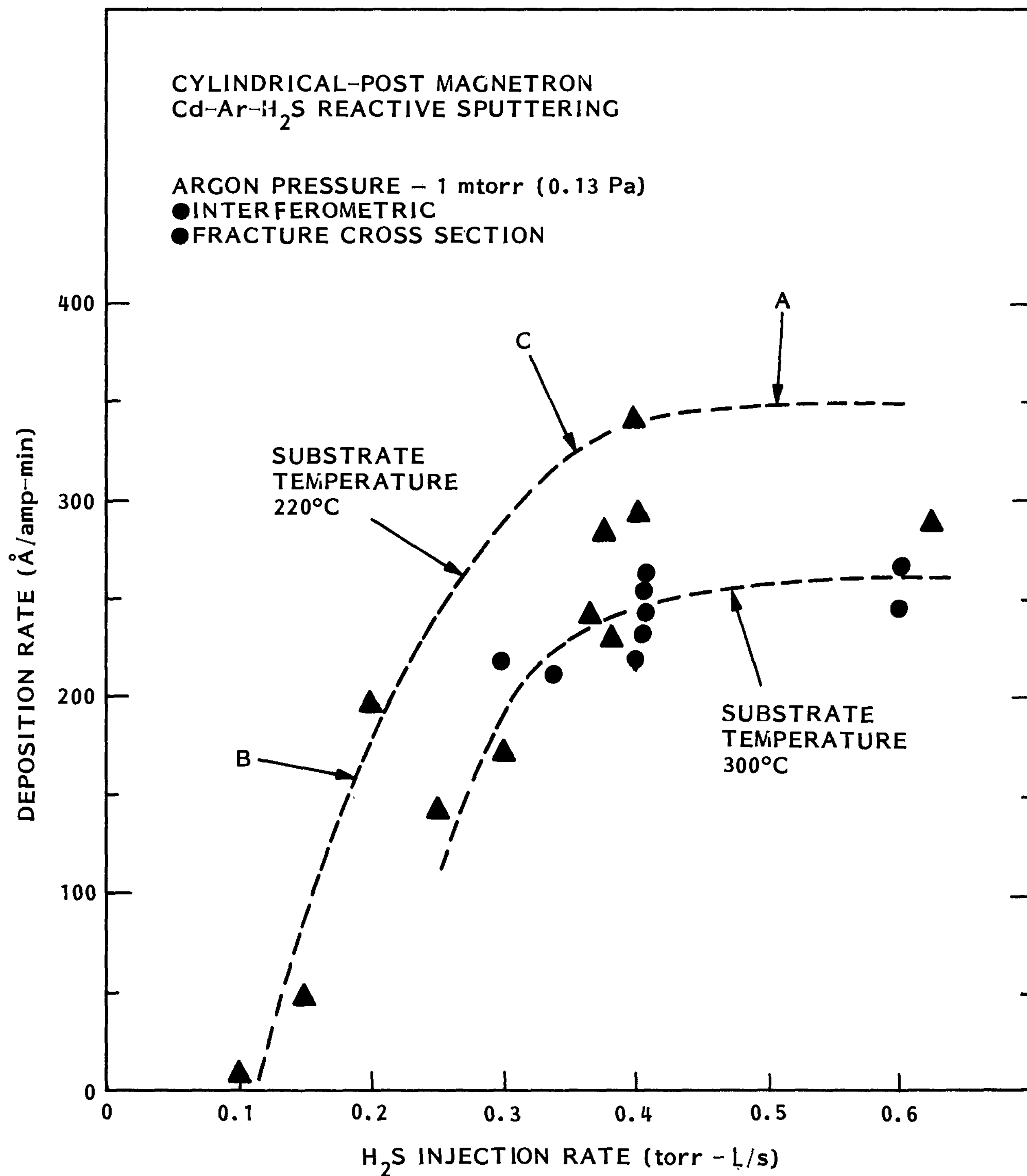

Fig. 12 Dependence of CdS Deposition Rate on H_2S Injection Rate and Substrate Temperature During Cylindrical Magnetron Reactive Sputtering. From Ref. 1

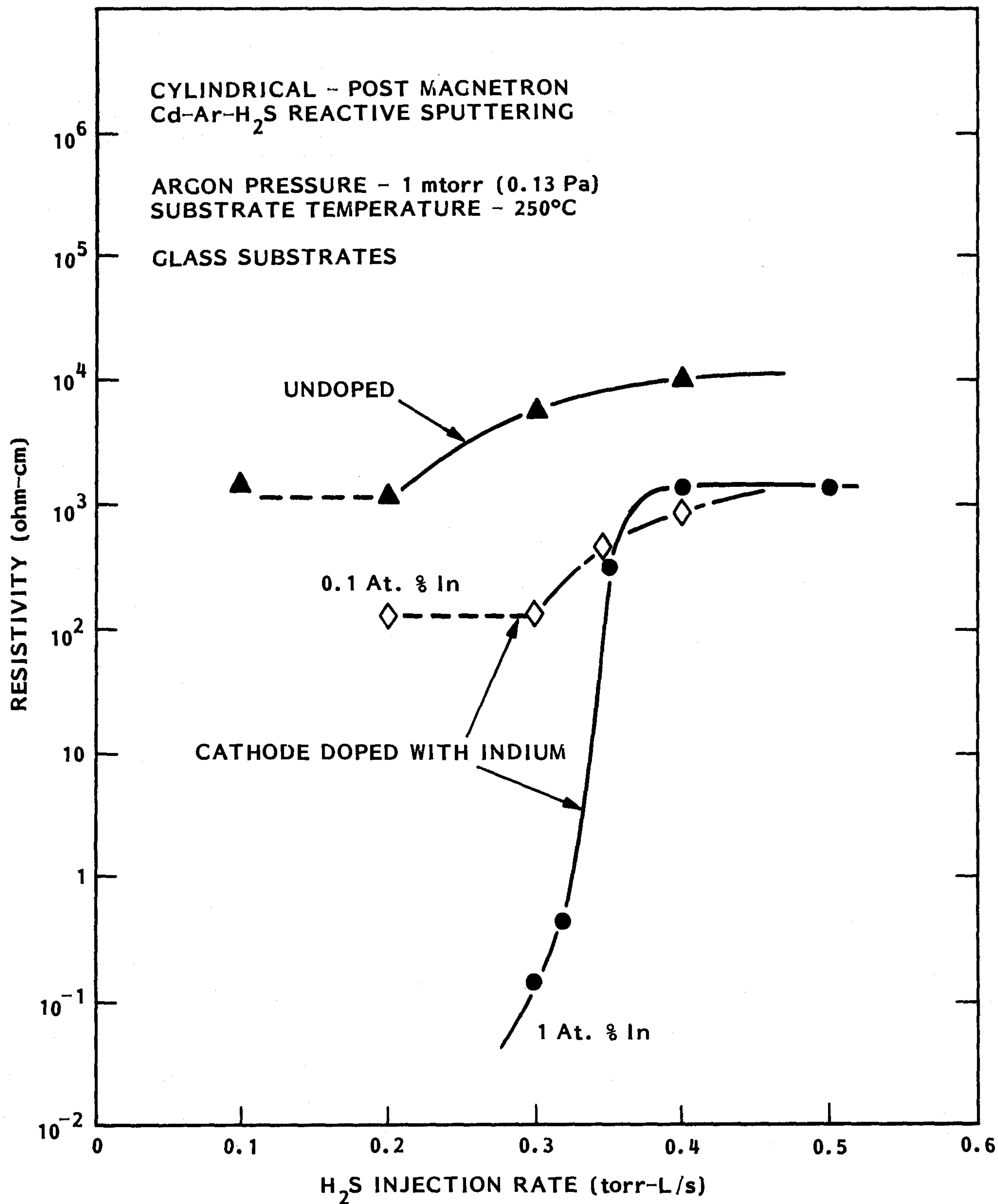

Fig. 13 Resistivity Versus H_2S Injection Rate for Reactively Sputtered CdS Coatings

the resistivity of undoped CdS from 10^4 to 10^3 Ω-cm; i.e., by an amount identical to that associated with a reduction in the steady state H_2S injection rate as shown in Fig. 13. The pulsed method was also used with the cathode doped with 1 at. % of In. Low resistivity (10^{-1} Ω-cm) coatings were obtained for average H_2S injection rates that would have yielded high resistivity (10^3 Ω-cm) coatings under steady state injection. This indicates that the pulsed injection method is in fact effective in reducing the Cd vacancy level.

Section 3
DEVICE-MATERIAL PARAMETER CHARACTERIZATION

3.1 SPECTRAL RESPONSE

The all-sputtered Cu_2S/CdS cell is a very planar structure as shown by the visibility of the interference fringes for both the CdS layer ($V_{CdS} \approx 0.10$) and the Cu_2S layer ($V_{Cu2S} \approx 0.13$) as shown in Fig. 14. The strong CdS interference, still visible with the Cu_2S overlayer, provides a convenient nondestructive measurement of CdS layer thickness.

The reflectivity of this structure is modeled as consisting of two components, a coherent reflectance component exhibiting interference phenomenon and an incoherent component. The coherent reflectance was obtained from standard transmission line formulas using the absorption coefficients and refractive indices for Cu_2S and CdS and a termination determined from the measured Nb reflectivity, R.

$$Z_L = \frac{1 - \sqrt{R}}{1 + \sqrt{R}}$$

The incoherent component was obtained by considering only power reflection, transmission, and absorption at each interface or in each region. Assuming 50% coherent and 50% incoherent, the calculated reflectivity is shown in Fig. 15. Two features are immediately evident: the calculation over emphasizes interference in the CdS layer and under estimates interference in the Cu_2S layer. The SEM photos in Figures 2 and 3 show that the CdS surface is textured laterally with a characteristic dimension the order of 1 μm, and vertically with a characteristic dimension the order of 0.2 μm. Thus we expect strong interference effects from multiple reflection within the quasi-planar Cu_2S layer but a significant loss of coherence on round-trip transit through the CdS layer. A calculation of interference in the Cu_2S layer only gives a better match

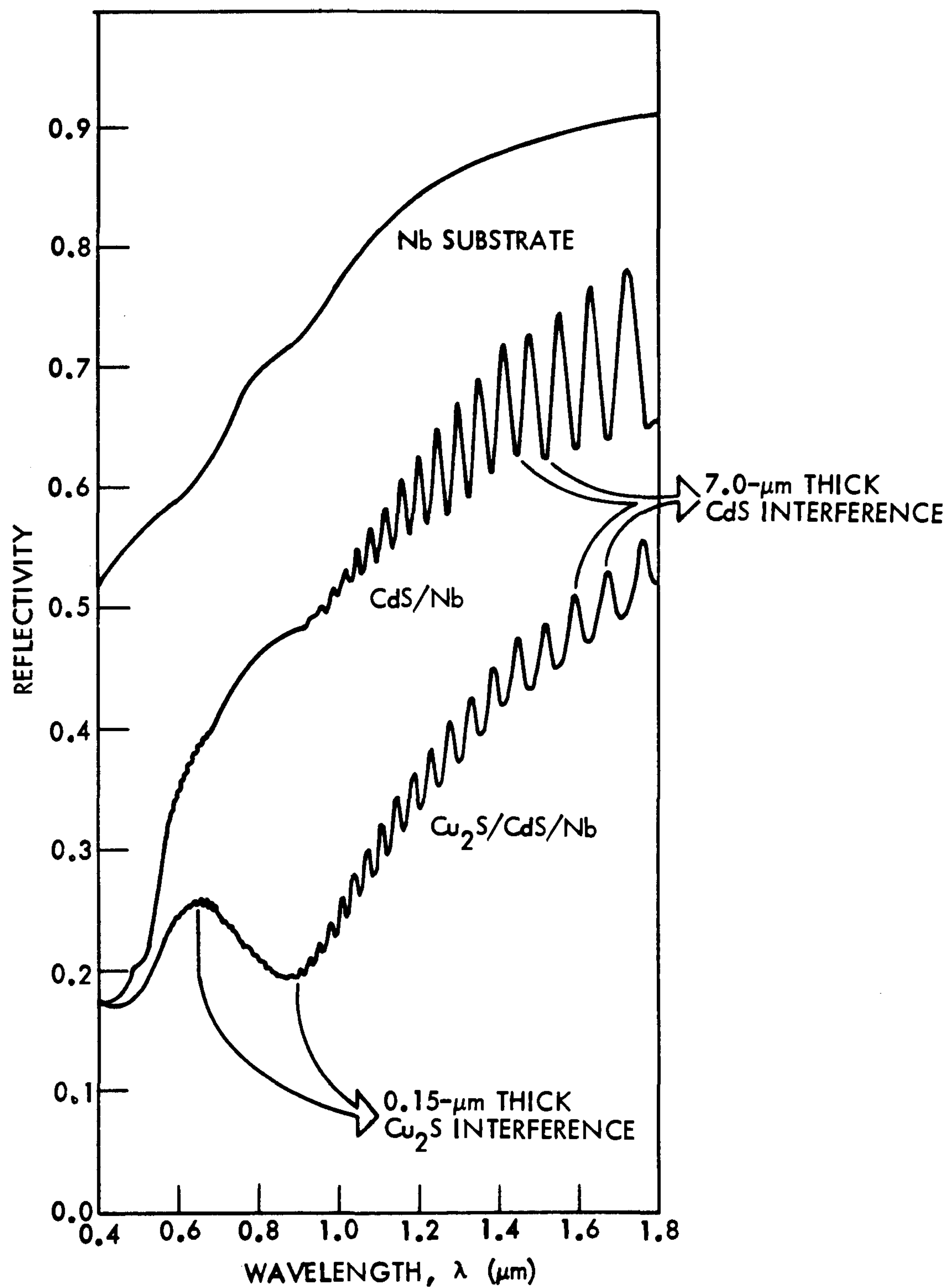

Fig. 14 Spectral Reflectivity of Successive Layers of Cu_2S/CdS/Nb Solar Cell Structure

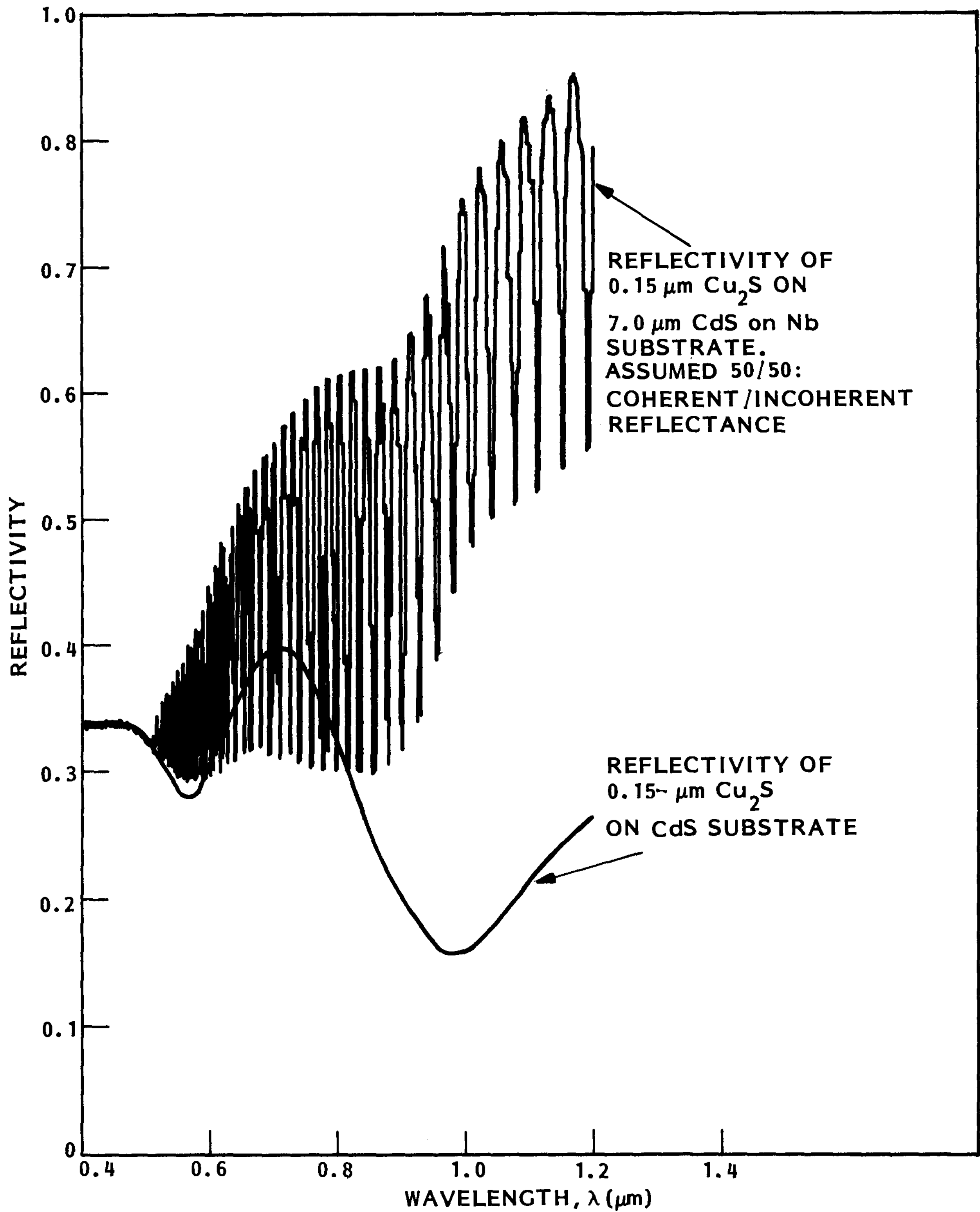

Fig. 15 Calculated Reflectivity of Cu_2S/CdS/Nb Solar Cell Structure and of Cu_2S/CdS Structure

to the observed reflectivity for $0.6 \leq \lambda \leq 1.2\ \mu m$. Therefore, an AR coating should be designed to maximize coupling into the Cu_2S layer without concern for interference effects within the CdS.

When the back surface reflectivity specific to Nb from Fig. 14 is introduced into the solar cell quantum efficiency Eq. (1)

$$\eta = \frac{\alpha L_n}{\alpha^2 L_n^2 - 1}\left[\frac{\alpha L_n (1 - R e^{-2\alpha t}) - (1 + R) e^{-\alpha t} \sinh \frac{t}{L_n}}{\cosh \frac{t}{L_n}} + \alpha L_n e^{-\alpha t} (R - 1)\right] \quad (1)$$

and integrated over the solar spectrum, we find the predicted maximum short-circuit current densities of Fig. 16 as a function of Cu_2S layer thickness. Also shown in Fig. 16 are the photocurrent densities previously calculated for perfectly reflecting and nonreflecting back surfaces (Ref. 1). Note that the nonideal ($R \neq 1$) reflectively of Nb only reduces J_L by 7 to 11% depending on L_n compared to a reduction of 21 to 28% for a completely nonreflecting ($R = 0$) back wall.

No correction for multiple pass interference is included in Eq. (1). However, significant interference is observed in Fig. 14. Hill and coworkers (Ref. 26) have shown that interference phenomena in planar cells can be used to significantly enhance cell response.

The spectral response of a cell is shown in Fig. 17. For comparison, the shape of the spectral response calculated from Eq. (1) is shown for the indicated parameters.

The calculation does not include multiple pass interference. Nevertheless, reasonable agreement is obtained for $0.51 < \lambda < 1.0\ \mu m$. The dip in short-circuit current on the long wavelength side of the CdS absorption edge was noted in early Cu_2S/CdS cell studies and recently studied by Robertson and Woods (Ref. 27).

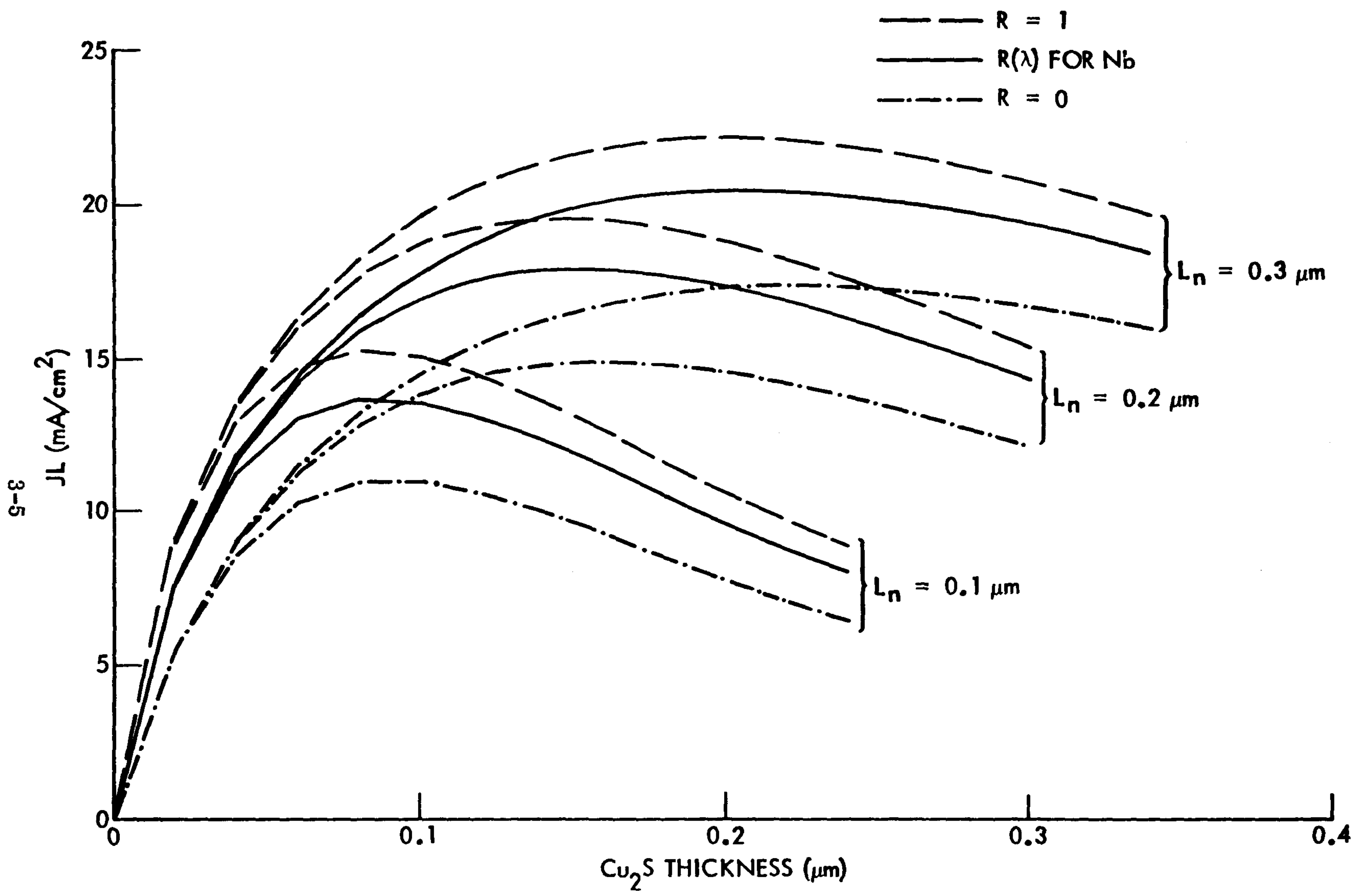

Fig. 16 Maximum Short Circuit Current Obtainable From Cu_2S Layer With Back Surface Reflectivity and Minority Carrier Lifetime as Parameters

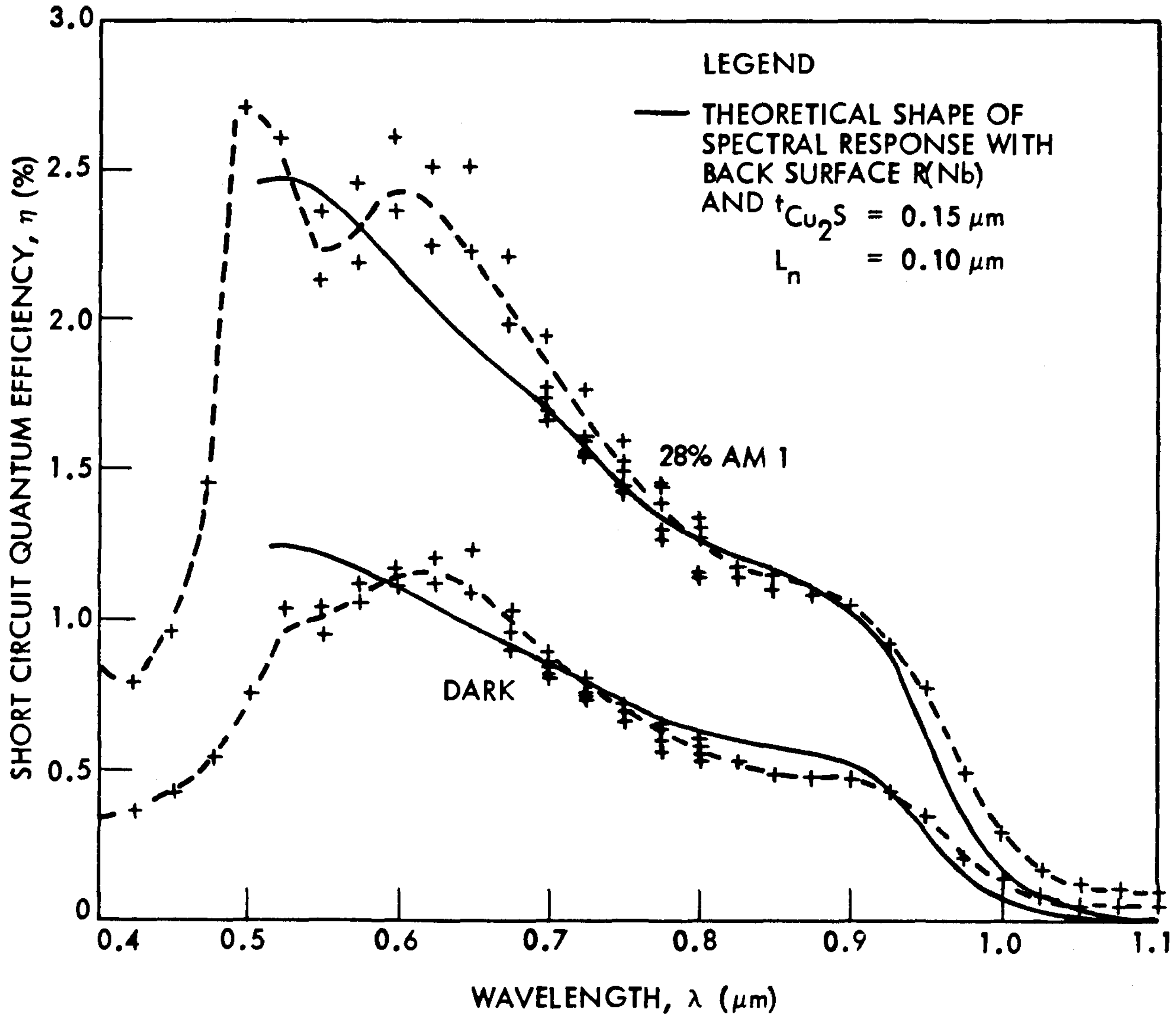

Fig. 17 Spectral Response of All Sputter Deposited CdS/Cu_2S Cell No. 824

The conclusions to be drawn from Figs. 16 and 17 and Table 2 are:

- Observed photocurrent is generated in the Cu_2S layer
- Junction carrier collection efficiency is, $\eta_j < 0.15$ to 0.25, depending on L_n when $J_{SC} \approx 3$ mA/cm^2

3.2 JUNCTION COLLECTION EFFICIENCY

Rothwarf's theory of field-aided junction collection efficiency (Ref. 6) predicts:

$$\eta_j = \frac{E_o}{\frac{S_j}{\mu} + E_o} \tag{2}$$

where, for a uniform effective donor dopant density, N_D^*, in the CdS adjacent to the junction,

$$E_o = \sqrt{\frac{2\,q\,N_D^*\,(V_D - V)}{\epsilon_r\,\epsilon_o}} \tag{3}$$

where V_D is the diffusion potential in the CdS and V is the nonequilibrium or external junction voltage.

For the low collection efficiency of all sputtered junctions to date,

$$S_j/\mu \gg E_o$$

and

$$\eta_j \approx \frac{\mu}{S_j}\sqrt{\frac{2\,q\,N_D^*\,V_D}{\epsilon_r\,\epsilon_o}}\left(1 - \frac{V}{V_D}\right)^{1/2} \tag{4}$$

which implies a nonsaturating reverse bias photocurrent until $E_o \approx S_j/\mu$. A linear relation between I^2 and V implied by Eq. (4) is commonly observed as shown for two cells in Fig. 18. The plot for Cell 653 is only taken to -0.3 V since an incipient reverse breakdown occurs at $V \approx 0.4$ V under AM 1 as may be seen from Fig. 1. While complete data were not taken on the cells examined to date to evaluate all of the quantities in Eq. (4) [or Eq. (2)], we estimate $2.4 \times 10^4 > S_j/\mu > 3.87 \times 10^3$ V/cm for Cell 653 and $7.8 \times 10^3 > S_j/\mu > 4.6 \times 10^3$ V/cm for cell 917. These numbers were based on N_D^*s obtained from van der Pauw measurements on CdS similar to that used in Cell 653 and the observed series resistance of the cell. C-V measurements under AM 1 illumination were used to determine N_D^* on cell 917. Junction efficiency was taken to be $J_{sc}/15.5$ which underestimates η_j. (See Tables 1 and 2.) These values of S_j/μ are comparable to those observed in good cells $S_j/\mu \approx 1.37 \times 10^3$ - 4.48×10^3 V/cm from Ref. (28). However, the interface electric field intensity is much too low.

To obtain low CdS bulk resistivity and maintain a high interface collection field, multilayer CdS/CdS:In structures as shown in Fig. 19 are being examined. The undoped or high resistivity CdS region is ~ 0.1 - to 0.5-μm thick. Cells were deposited with 1.0%-at In, so that when the space charge layer expanded through the undoped CdS region, the heavily doped CdS region prevented further space charge layer widening under reverse bias. The predicted C-V behavior was observed as shown in Fig. 20. This cell was deposited with a 0.5-μm-thick undoped CdS region which agrees with the observed saturation of space charge layer width at $W \approx 0.48$ μm. For a stepwise variation in doping, the functional form of E_o versus V changes from that given in Eq. (3) for uniform doping to:

$$E_o = \frac{2V_D}{W_1}\left(1 - \frac{V}{V_D}\right)^{1/2} \qquad \text{for } V \geq V_D\left(1 - \frac{W_0^2}{W_1^2}\right)$$

$$= \frac{W_0}{W_1^2} V_D \left(2\frac{W_0}{W_1} - 1\right) + \frac{V_D}{W_0}\left(1 - \frac{V}{V_D}\right) \text{ for } V \leq V_D\left(1 - \frac{W_0^2}{W_1^2}\right)$$

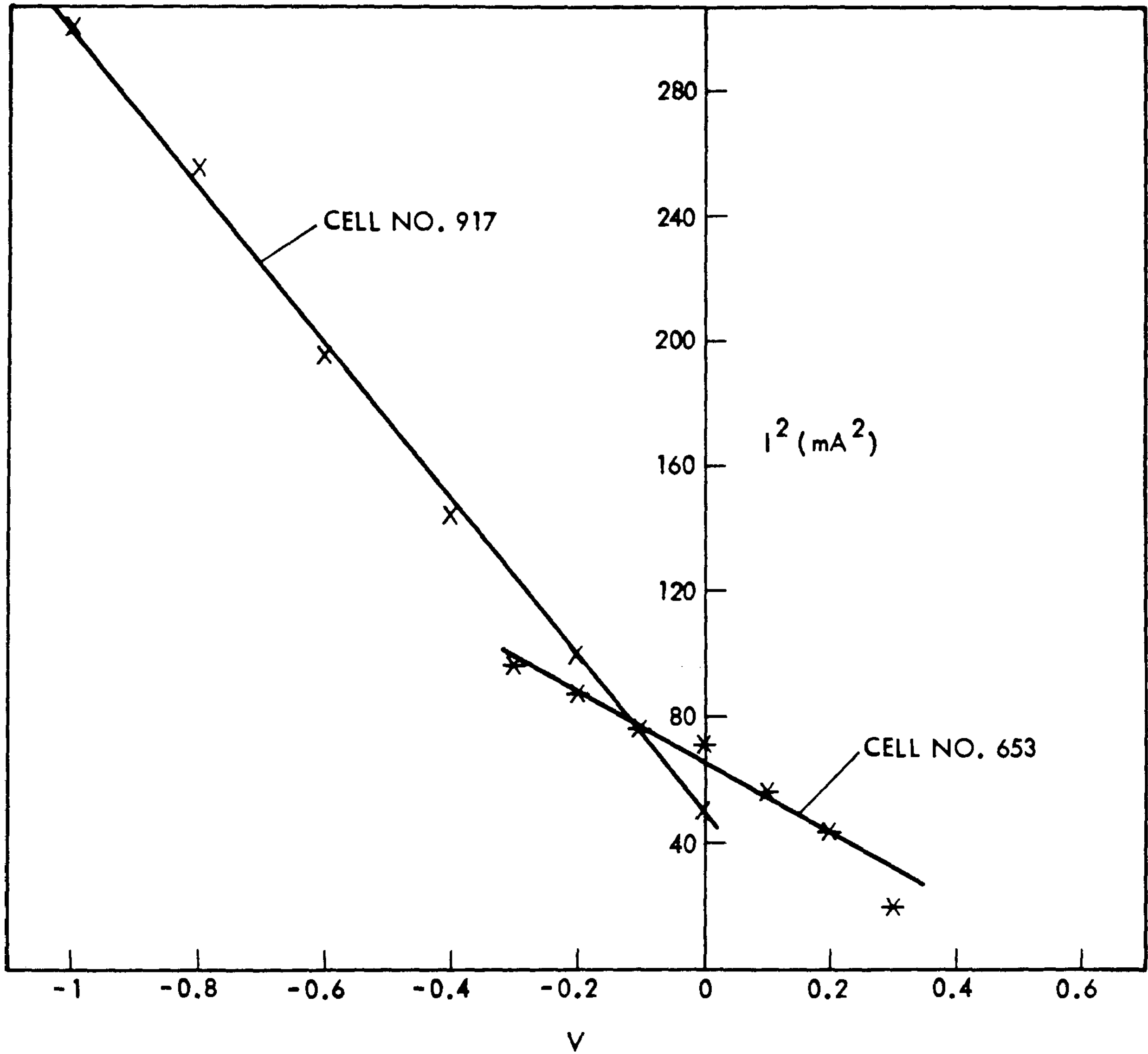

Fig. 18 Collected Photocurrent Squared Versus Device Voltage Under AM 1 Illumination for Two Cells

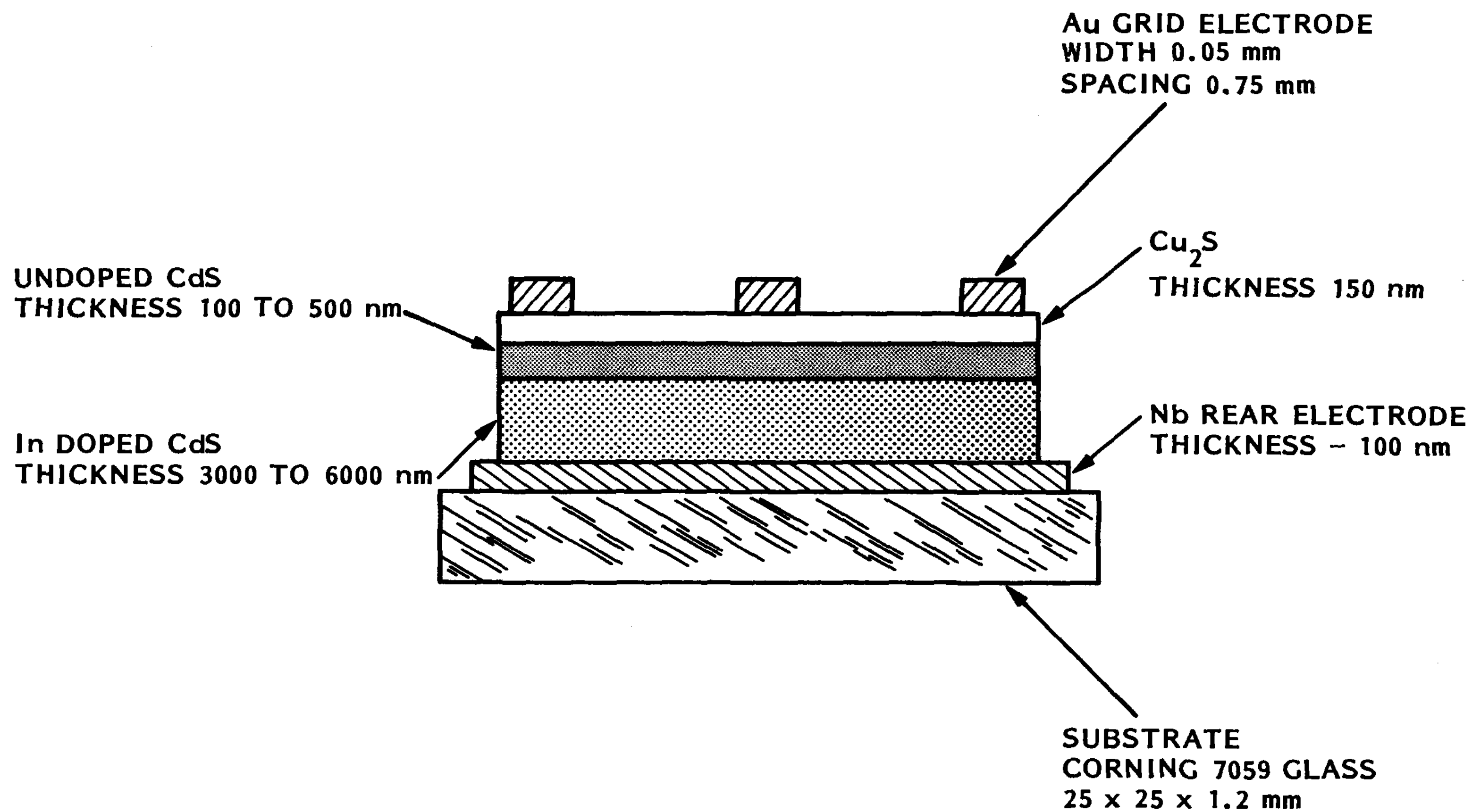

Fig. 19 General Configuration of Multilayer CdS Sputter-Deposited Solar Cell

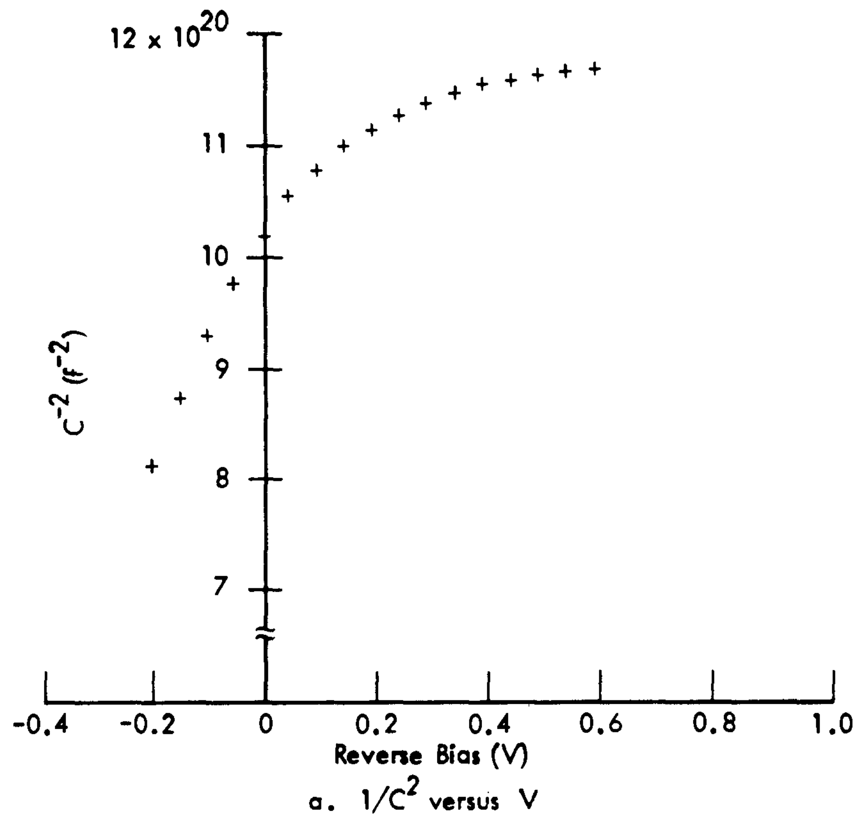

a. $1/C^2$ versus V

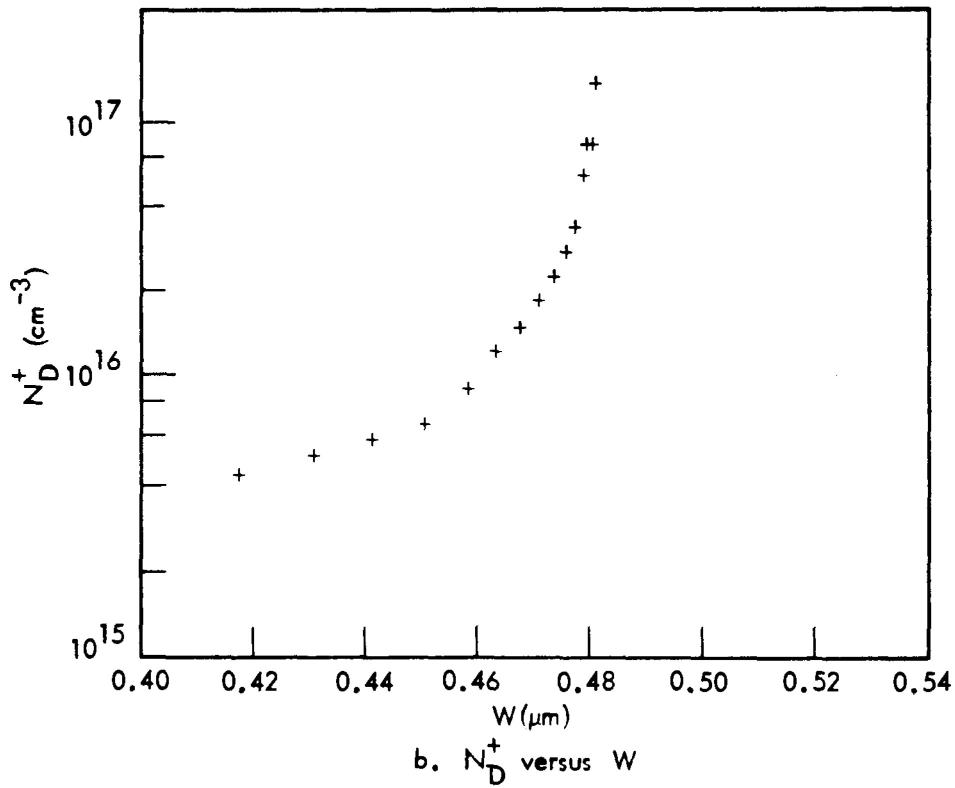

b. N_D^+ versus W

Fig. 20 Capacitance-Voltage and Corresponding Ionized Impurity Concentration Versus Depth for Cu_2S/CdS/CdS:In Solar Cell Structure

where $W_1 = \sqrt{\dfrac{2\,\epsilon_r \epsilon_o V_D}{q\,N_D^*}}$ and W_o is the width of the lightly doped region.

The I-V characteristic of a solar cell with a doping level discontinuity is shown in Fig. 21. Note the linear I-V characteristic under AM 1 illumination for $V < -0.1$ V under AM 1 illumination.

For In-doped CdS and composite or multilayer structures, the effects of heat treatment during junction activation are expected to be different from conventional cells. Shiozawa et al. mentioned the different Cu diffusion, solubility, and photoconductivity for In-doped cells vis-á-vis undoped cells (Ref. 5). We have observed a great variability in heat treatment effects on our cells to date. Figure 22 shows the development of cell characteristics similar to that described by Te Velde (Ref. 29). However, some cells rapidly develop a very high resistance during heat treatment. This was the case of Cell 917 described previously.

A more complete picture of the electric field at the junction, and its development with heat treatment, is provided by capacitance versus voltage studies made at the University of Delaware Institute of Energy Conversion (IEC) on cells with evaporated CdS layers and our measurements on sputter-deposited cells. Table 6 compares depletion layer widths deduced from these capacitance measurements for cells in their as-fabricated state, after heat treatment, and during subsequent exposure to solar illumination. The as-deposited depletion layer thicknesses are consistent with predictions made using

$$W = \sqrt{\frac{2\,\epsilon_r \epsilon_o (V_D - V)}{q\,N_D^*}}$$

and measured donor densities. The sputtered cell data are for cells with the composite n^+/n structure shown in Fig. 19. The depletion layer implied by the capacitance measurements corresponds, as would be expected, to the width of the undoped layer and therefore confirms the control which was maintained during the deposition.

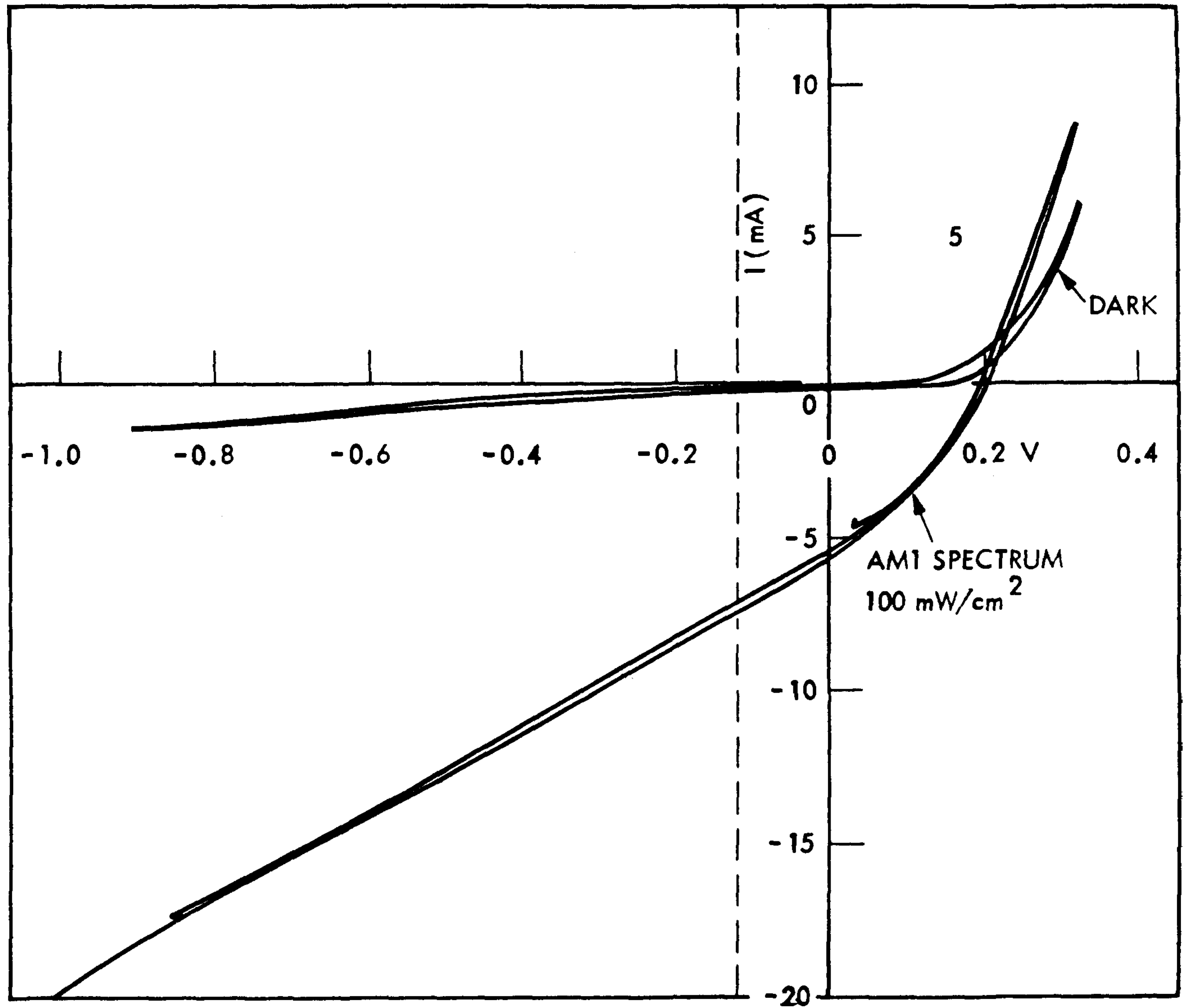

Fig. 21 I-V Characteristic of Cell No. 914 Which Shows Linear I-V Relation for V < -0.1

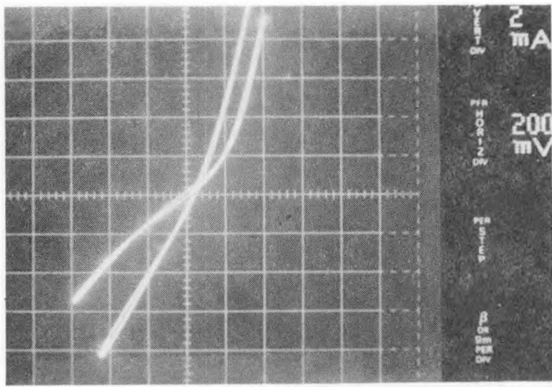

a. Unannealed

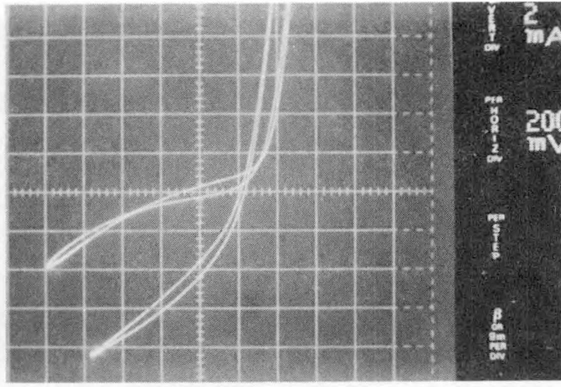

b. 2 min at 190°C

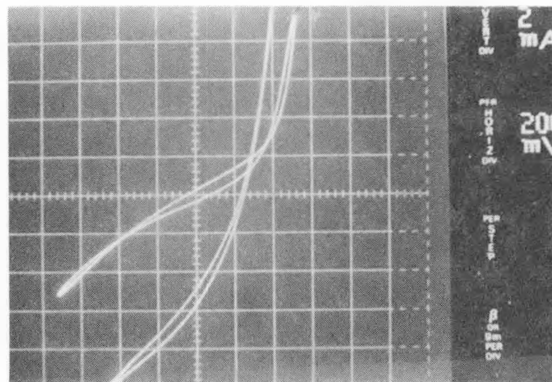

c. 4 min at 190°C

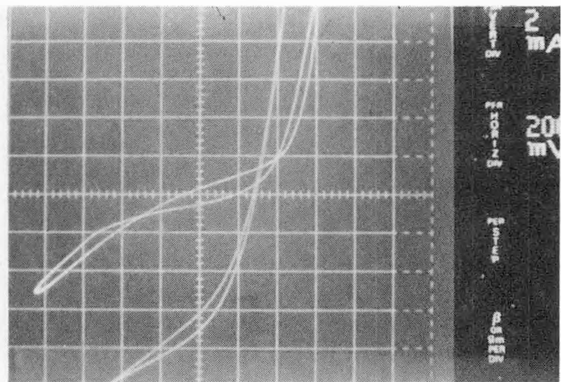

d. 6 min at 190°C

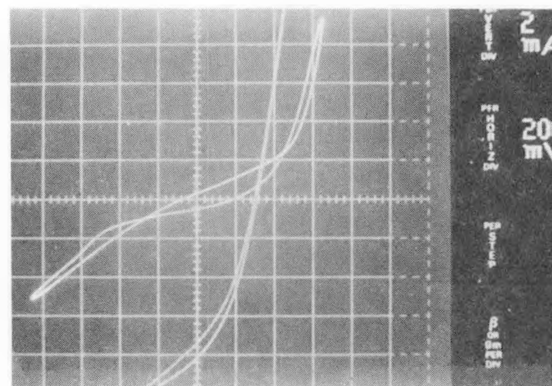

e. 8 min at 190°C

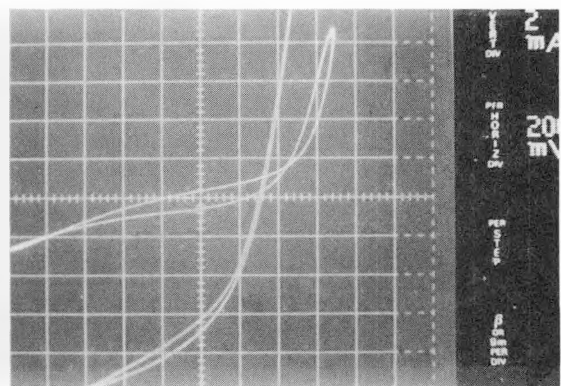

f. 10 min at 190°C

Fig. 22 Development of Dark and AM 1 I-V Characteristic With Annealing at 190 C in H_2. Cell No. 824

During heat treatment the depletion layer widths increased in both cases and, in the sputtering case, extended to the entire thickness of the cell. The significant observation is that under solar illumination the depletion layer width in the evaporated cells decreased by approximately an order of magnitude, while in the sputtered cells it did not.

Table 6
DEPLETION LAYER WIDTHS

	Evaporated CdS Wet process Cu_2S Inst. Energy Conv.	Sputtered CdS Sputtered Cu_2S Telic/Lockheed
As deposited	$\sim 0.1\ \mu m$	$\sim 0.5\ \mu m$
After heat treatment	$\sim 10\ \mu m$	$\sim 5.2\ \mu m$
Under solar illumination	$\sim 0.17\ \mu m$	$\sim 3.0\ \mu m$

Finally, we note that, under forward bias, the I-V characteristics of the Cu_2S/CdS cells appear to be described by a TFL space charge-limited current flow (Ref. 3) as shown in Fig. 23 rather than the conventional diode equation. This type of I-V characteristic has also been observed on conventionally fabricated Cu_2S/CdS (Ref. 30). It has also been observed in other pn-heterojunctions (Ref. 31). The two different fabrication processes referred to in Fig. 23 are the off-stoichiometry doping of Cell 653 (see also Fig. 1 and 18) and the composite CdS structure of Cell 804 (see Fig. 20).

3.3 HYBRID PROCESS CELLS

As mentioned in the discussion of Table 4, it appears that the main problem associated with the all sputter-deposited Cu_2S/CdS solar cell is in the CdS layer. Further evidence for this is the problem of resistivity control (see section 2.3) and interfacial field development (see section 3.2). To further evaluate sputter-deposited CdS, a set of CdS films was sent to the University of Delaware Institue of Energy Conversion

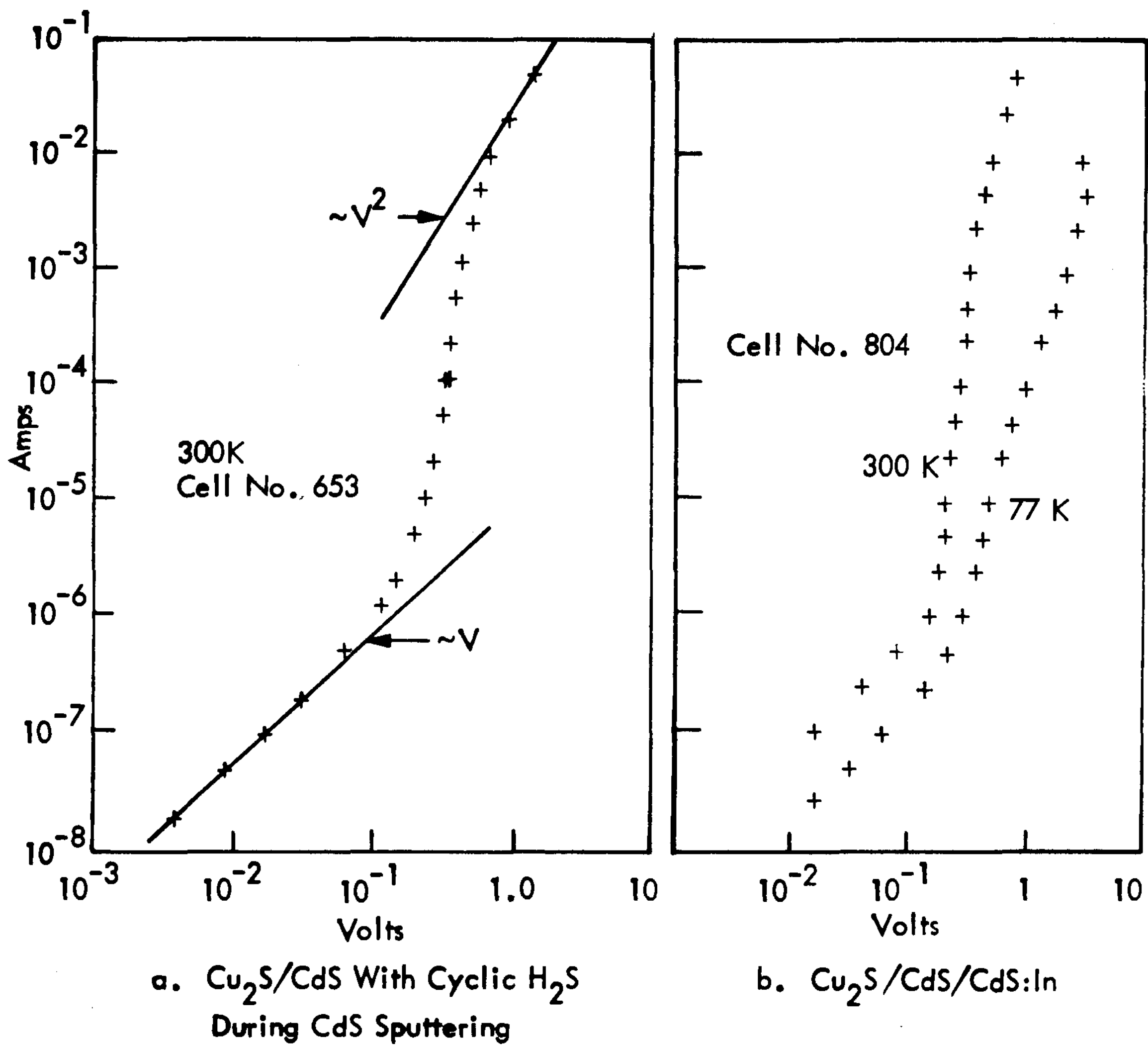

Fig. 23 Current-Voltage Characteristics of Cu_2S/CdS Cells With CdS Deposited by Two Different Processes[2]

(IEC) for application of Cu_2S coatings by the CuCl "wet" process and "dry" process. Au grids were sputter deposited at Telic and measurements were then performed at LMSC.

A summary of cell preparations is given in Table 7 along with measurements on the as-deposited cells. The wet processed heterojunctions were formed at IEC by first texturing the CdS coatings, using a 5- or 10-s immersion in 25% (by volume) HCl at 60 C, and then dipping them in a CuCl solution for 10 sec to yield a Cu_2S coating thickness of approximately 3000A. Dry process heterojunctions were formed by evaporating enough CuCl to react to an approximate thickness of 2500A. No HCl texturing was used on these samples. The wet process Cu_2S resulted in high shunt conductance or shorts in all individual grid lines. The dry process Cu_2S resulted in diode characteristics (with a few shunts and one short). Some photovoltaic response was obtained in all of the as-prepared samples except 935. The measurements given in Table 7 are for a single grid line only which implies collection of photocurrent from a rather small junction area.

Sample 964 was masked to expose an area of 0.6 cm^2 around a single grid line. This resulted in $Js^c \simeq 4.1$ mA/cm^2 and $Vo^c \simeq 0.42$ volts with no sign of soft reverse characteristics under illumination. Heat treatments were performed on Cells 964 and 967 in $N_2/20\%$ H_2 at 150 C. Development of solar cell characteristics of a function of heat treatment is given in Table 8. The cell areas used were the "good" areas as determined from preliminary individual line measurements.

The I-V characteristic of Cell 967 after the first hour of heat treatment is shown in Figure 24. The significant dark shunt conductance was characteristic of all hybrid process cells. Note that the reverse bias illuminated characteristic is nearly a parallel displacement of the dark characteristic. This is to be contrasted with the region of reverse bias positive curvature characteristic of the all-sputter-deposited cells to date. (See Figs. 1 and 22). The later characteristic was ascribed to a field-dependent junction photocurrent collection efficiency as described in section 3.2. The hybrid process cells formed on undoped sputter-deposited CdS appear to have significantly different characteristics from the all sputter-deposited cells although this conclusion is very tentative, being based on only two devices.

TABLE 7

CELLS WITH Cu_2S APPLIED BY INSTITUTE OF ENERGY CONVERSION

Summary of Preparation

	CdS Deposition				Cu_2S Deposition			
Sample	Material	Temp.	H_2S	Thickness	Process	Textured time	Dip time	Thickness
934	Cd-0.1%In	250 C	3 m Torr	~11 μm	dry	-	-	0.25 μm
935	"	"	"	"	wet	5 s	10 s	0.30 μm
964	Cd(6-9's)	250 C	3 m Torr	~8 μm	dry	-	-	0.25 μm
965	"	"	"	"	wet	10 s	10 s	0.30 μm
967	Cd(6-9's)	250 C	4 m Torr	~5 μm	dry	-	-	0.25 μm
969	"	"	"	"	wet	10 s	10 s	0.30 μm

Summary of Measurements on "as-deposited" Cells

Sample	Isc (mA)	Voc (Volt)	COMMENTS
934	0.25	0.02	High shunt conductance at one end of grid array
935	-	-	All grids shorted to substrate
964	2.8	0.42	High shunt conductance at one end of grid array
965	1.8	0.13	All grids exhibit high shunt conductance
967	2.3	0.32	Grids 1, 19, and 30 high shunt cond.; 31 shorted
969	0.26	0.02	All grids exhibit high shunt conductance

Table 8

HEAT TREATMENT OF HYBRID PROCESS CdS/Cu_2S SOLAR CELLS

Cell No. and Area	Cumulative Time at 150 C in N_2/H_2	V_{oc} (V)	J_{sc} (mA/cm^2)	FF	Efficiency (%)
964	0	0.23	3.8	-	-
$A = 3.5\ cm^2$	4	0.38	4.29	-	-
	20	0.30	2.85	-	-
967	0	0.32	-	-	-
$A = 2.76\ cm^2$	1	0.40	6.9	0.43	1.18
	2	0.432	6	-	-
	4	0.41	5	0.33	0.68
	6	0.33	3	-	-
	8	0.30	2.6	-	-

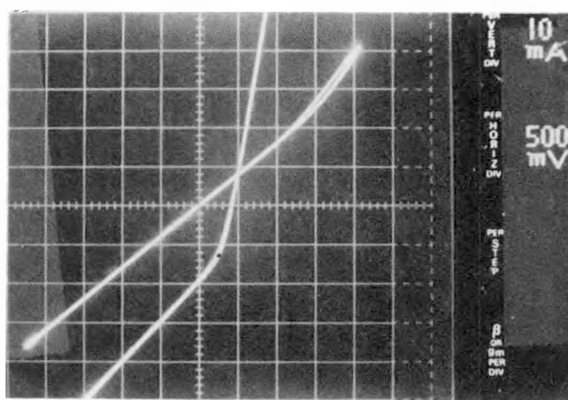

Fig. 24 Volt-Ampere Characteristic of Hybrid Process Cell 967 in the Dark and Under AM 1 Illumination

3.4 CELLS FROM MODIFIED SPUTTER DEPOSITION SYSTEM

All films and cells described previously were deposited in a multicathode magnetron reactive sputtering system configured as shown schematically in Fig. 25. Three features of this system resulted in problems with deposited material and/or device characteristic control and one feature resulted in operational inconvenience. These features were:

(1) Cu_2S deposition over edge of CdS
(2) CdS film annealing prior to Cu_2S deposition
(3) Chamber wall effects on deposited material composition
(4) Long turnaround time between deposition runs

Cu_2S deposition follows CdS deposition by simply rotating the substrate holder from the Cd cathode to the Cu cathode and switching the discharge from the Cd cathode to the Cu cathode. As a result, the Cu_2S deposition area completely covers the CdS deposition area and some Cu_2S scattering over the edge of the CdS film edge occurs. When the Cu_2S is low resistivity, the Cu_2S may short to the substrate resulting in the shunted characteristic as shown in Fig. 8.

CdS deposition is carried out at a substrate temperature of T_s = 250 C while Cu_2S deposition is carried out at T_s = 150 C. Thus a cooling time delay occurs between CdS deposition and Cu_2S deposition. With the original substrate holder, the minimum cooling time was 12 min. From the discussion in section 2.3 of Cd vacancy effects and the tendency toward self-compensation in CdS without an overpressure (or incident flux) of Cd, this time interval may be adequate to change the as-deposited film composition. Note the heat treatment effects in Fig. 22 which occur on a time scale of minutes at 190 C. It is desirable to be able to quench-in the as-deposited CdS characteristics for complete material parameter control.

Deposition conditions for Cu_xS layers deposited during most of the heterojunction studies using the multisource deposition apparatus have differed from those used in a preliminary study in the following ways.

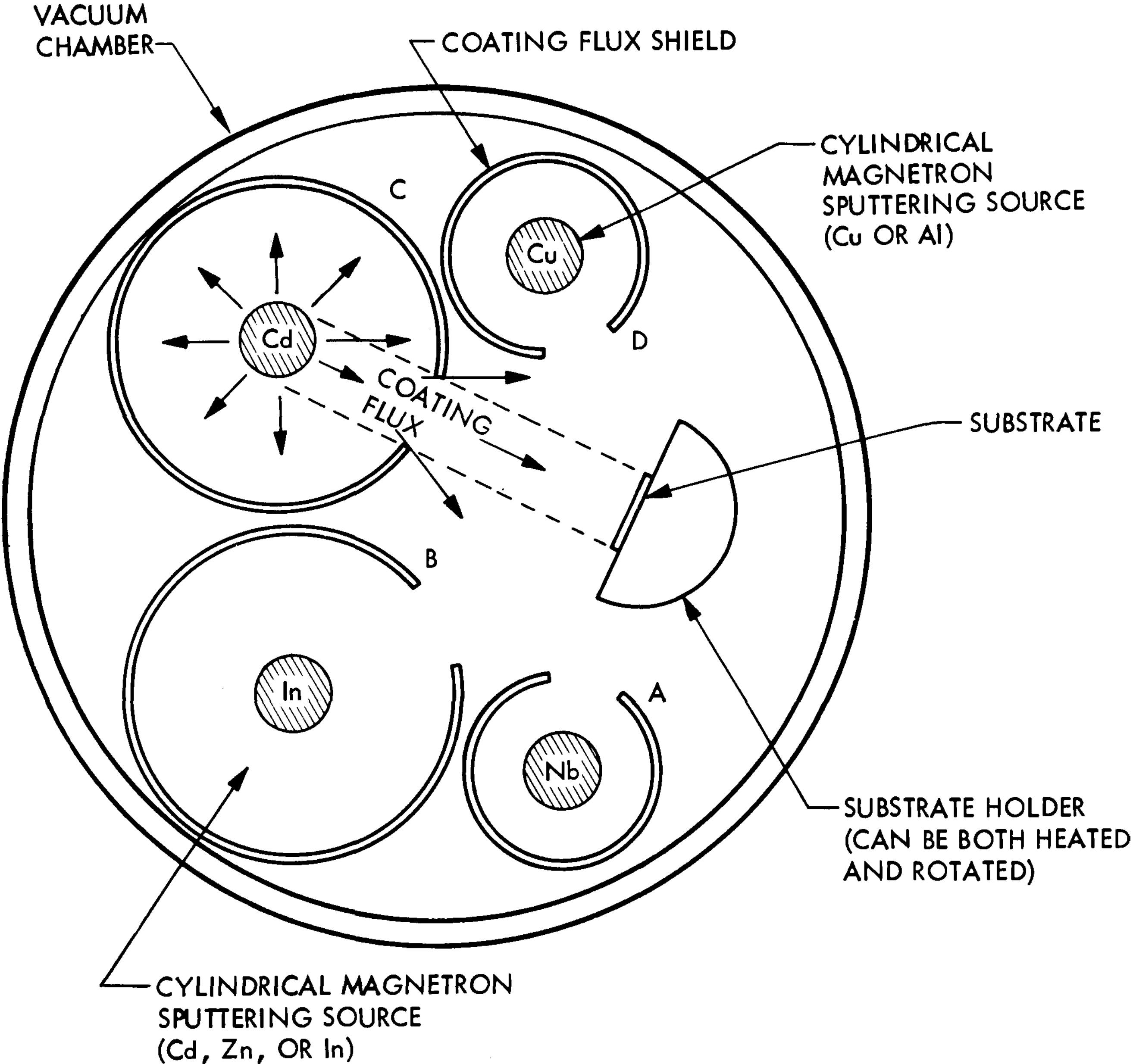

Fig. 25 Multicathode Magnetron Reactive Sputtering System Schematic for Sequential Deposition of Multilayer Films

(1) Coatings were deposited onto CdS rather than glass substrates
(2) Substrate temperature was 150 C (the higher substrate temperature was used to minimize the time delay between the CdS and Cu_xS depositions and to assist in formation of the junction)
(3) Extensive conditioning of the cathode was not used between the CdS and Cu_xS depositions

Several inconsistencies were encountered between the resistivities of Cu_xS coatings deposited in the heterojunction work and the trends previously determined. Thus, at the start of the present program, a procedure was adopted whereby the Cu cathode was operated in Ar for 5 min to clean the surface and then in H_2S for 3 min to condition the surface before opening the chamber and loading the substrates. During cell fabrication, following the CdS deposition, the Cu cathode was again conditioned by operating in H_2S for 4 min with the substrates shielded. The resulting coatings were found to have low resistivities over injection rates ranging from 0.07 to 0.175 torr-L/s, even though the deposition temperature was 150 C. When the in situ conditioning step was discontinued, the expected high resistivity coatings were deposited. The cause of the low resistivity coatings was tentatively attributed to heating of the cathode shield and the release of sulfur-bearing species which effectively increased the H_2S injection rate.

Additional work was conducted with particular emphasis on the role of the CdS substrate and those aspects of the Cu_xS deposition procedure that can be expected to be applicable to the modified apparatus. Thus coatings have been deposited onto predeposited CdS layers, 500-nm thick, at substrate temperatures of 50 C and 150 C. The circular shield was removed from the Cu source (see Fig. 25) to approximate the modified apparatus, and particular attention has been given to the effects of cathode sputter cleaning and conditioning, since the modified apparatus will permit effective incorporation of these procedures. The following has been observed.

(1) The basic resistivity versus H_2S injection rate relationship previously obtained for glass substrates has been confirmed for coatings deposited onto CdS. Thus at moderate H_2S injection rates, coatings with high

resistivities were obtained at substrates temperatures of 50 C and 150 C. Above a critical injection rate of about 0.14 torr-L/s, coatings with low resistivities were obtained at 50 C. At high injection rates, low resistivities were also found for the 150 C coatings. The data are summarized schematically in Fig. 26. In all cases, the cathode was sputter-cleaned in Ar and pre-conditioned just prior to depositing the Cu_xS coating, by operating for several minutes at the prescribed H_2S injection rate with the substrates shielded.

(2) With one exception (see Item 4 below), regardless of the deposition conditions, those Cu_xS coatings with high resistivities possessed a relatively high density of Cu nodules, while those with low resistivities did not. The nodule diameter was typically about 2 μm. The nodule surface density was typically about $5 \times 10^6/cm^2$, decreasing slightly with increased H_2S injection rate.

(3) The required Cu_xS coatings are sufficiently thin so that the amount of sputtering required to deposit the coatings is small compared to that amount which is required to reach a state of equilibrium on the cathode and shield or chamber wall surfaces. Consequently the system can have a memory of previous deposition conditions, or can undergo a drift when an attempt is made to operate under fixed conditions. This is believed to be the cause of two departures which were seen from the data shown in Fig. 26. In one case a series of Cu_xS coatings were deposited at 150 C with the cathode surface in the state which existed following a previous set of cell depositions. The resistivities were low over H_2S injection rates of from 0.05 to 0.2 torr-L/s, even though the cathode was pre-conditioned by sputtering in the desired Ar-H_2S mixture for 4 min prior to exposing the substrates. Consistent results were obtained in subsequent work after the cathode was extensively sputter-cleaned in Ar. In a second case, a high rather than the expected low resistivity was obtained in a 50 C coating deposited at a high H_2S for 4 min. The solution to these unwanted variations is to suitably sputter-clean and condition the cathode

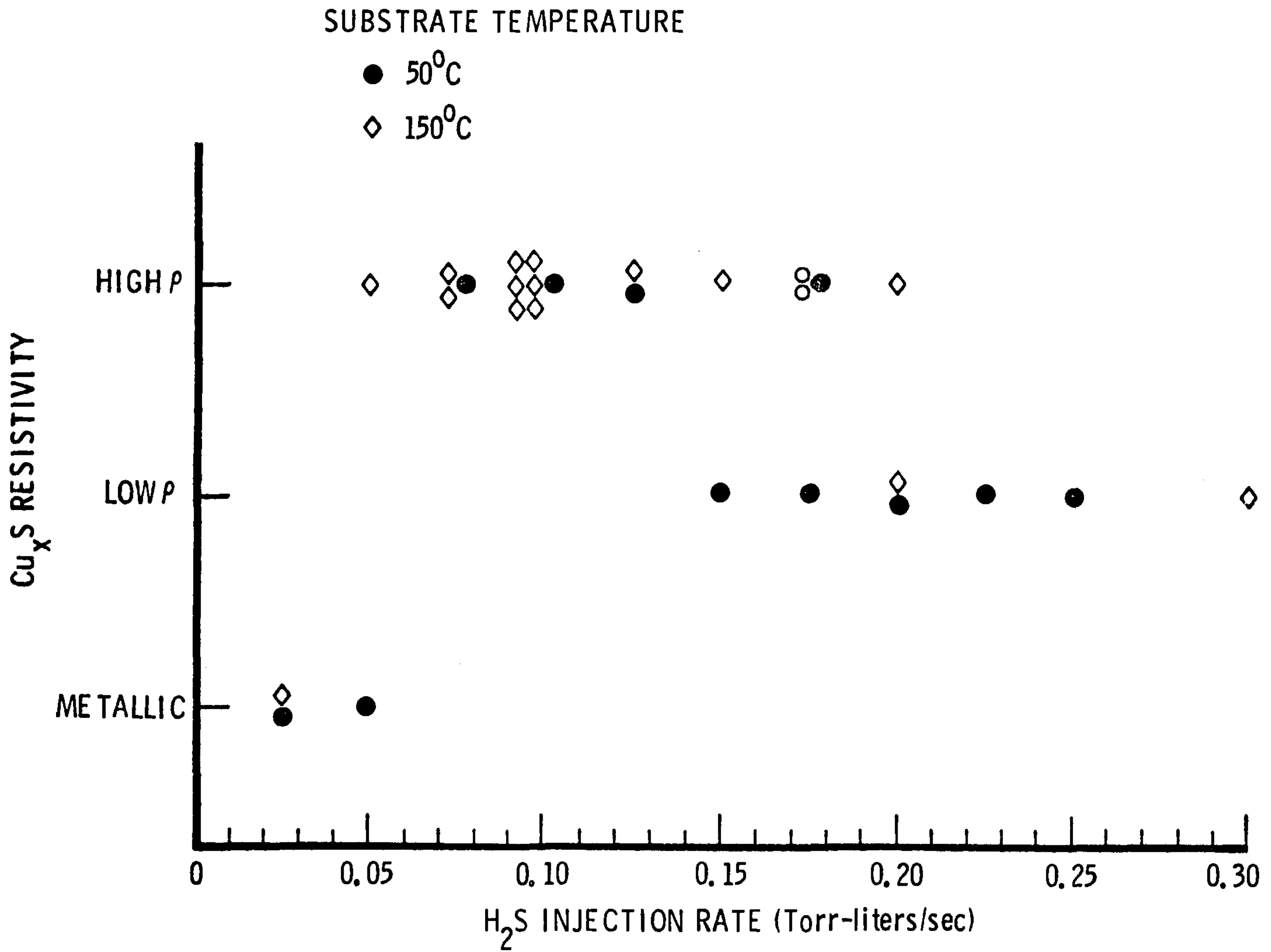

Fig. 26 Schematic Representation of Dependence of Resistivity on H_2S Injection Rate for Coatings Deposited Onto CdS

for a sufficient length of time before each deposition. It will be possible to conveniently perform this operation in the modified apparatus.

(4) The dependence of the Cu_xS coating properties on the state of the cathode and wall surfaces at the start of deposition raises the possiblity of forming coatings under combinations of conditions not shown in Fig. 26, by conditioning the cathode under one set of conditions and depositing the coating under another. In one case this procedure provided a high resistivity coating with an almost negligible density of Cu nodules. Additional work is required to explore the feasibility of this approach.

It was necessary to expose the entire sputter chamber to atmospheric pressure to remove and reload substrates. Overnight pumping was then required to adequately remove water vapor adsorbed on chamber surfaces. As a result, only one run per day was possible. Even with overnight pumping, some irreversible wall chemistry could occur, resulting in modified film and device characteristics.

The modified sputter deposition system is configured as shown schematically in Fig. 27. Specifically, this system is designed to eliminate the problems described above by:

(1) Installing a movable mask to restrict Cu_2S deposition at the cell edge
(2) Redesigning the substrate holder to permit rapid cooling of the substrates following the CdS and prior to the Cu_2S depositions
(3) Reconfiguring cathode shielding to reduce the shield surface area adjacent to the sputtering sources and substrates
(4) Installing a vacuum interlock so that substrates can be inserted without exposing the cathode and shield surfaces to the atmosphere

The modified system was placed in operation at Telic Corp. near the end of this contract period. After a series of shakedown runs to establish deposition parameters for CdS and Cu_2S individually, three complete cell deposition runs were performed with various CdS layers as indicated in Fig. 28. Also shown in Fig. 28 are corresponding single grid I-V characteristics typical of each cell type. Only the cell with

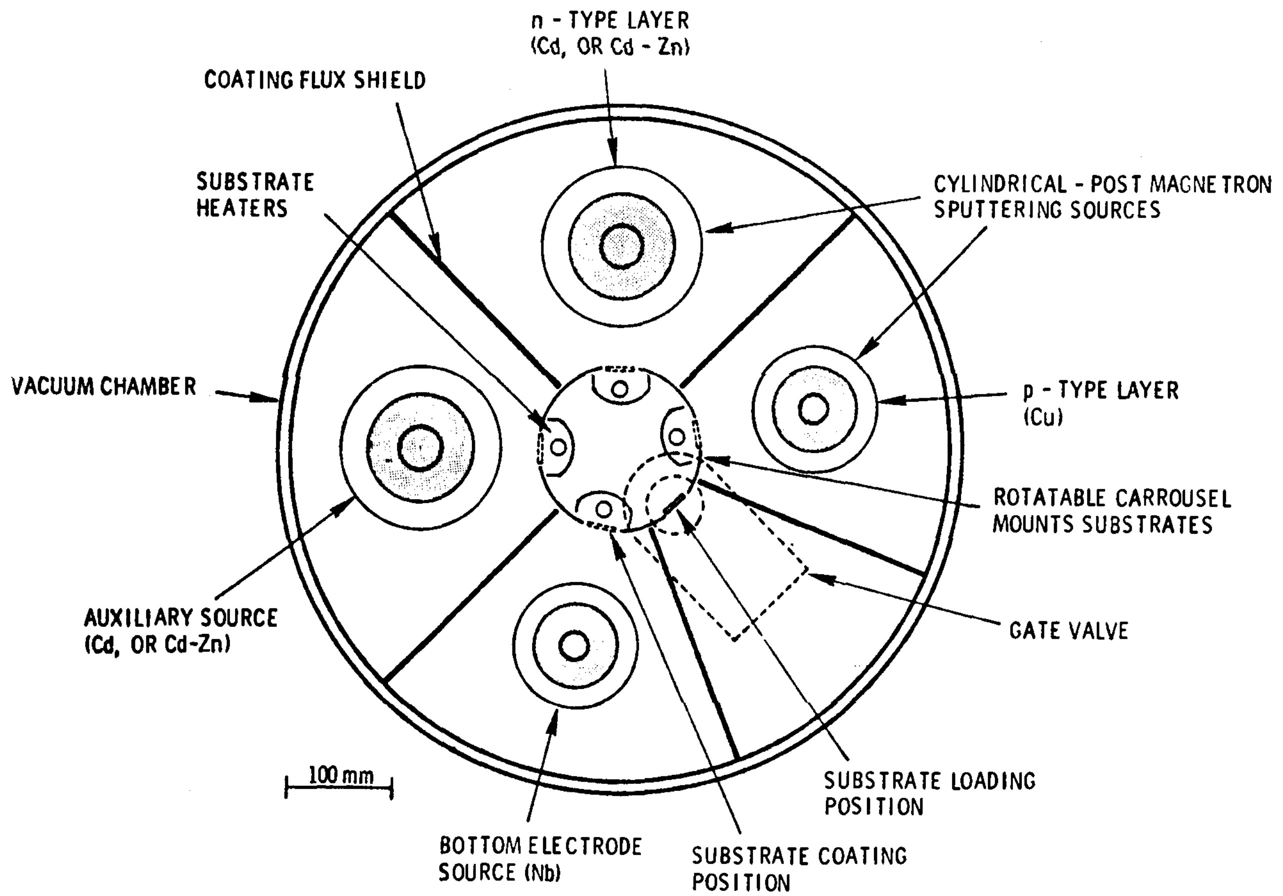

Fig. 27 Schematic Diagram of Modified Multisource Deposition Apparatus

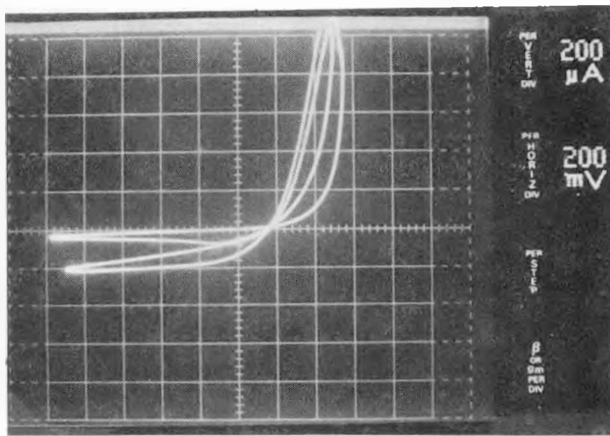

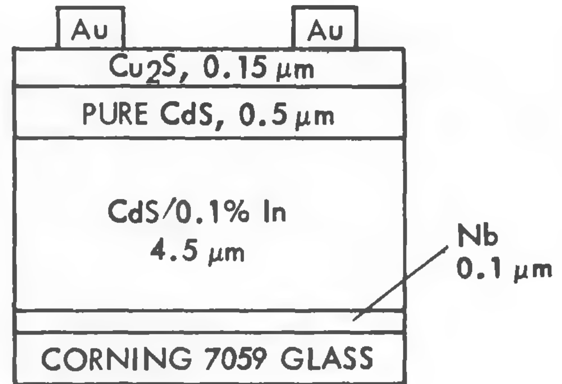

a. CELL #1181

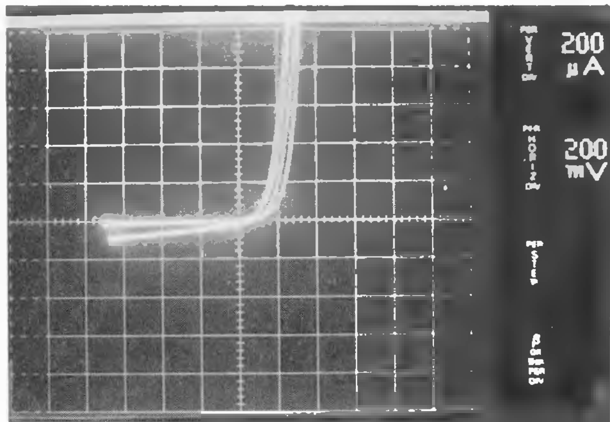

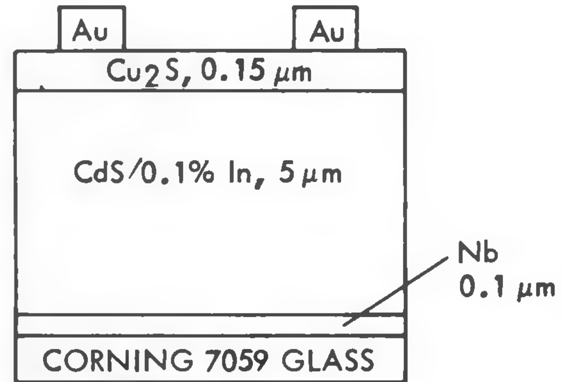

b. CELL #1175

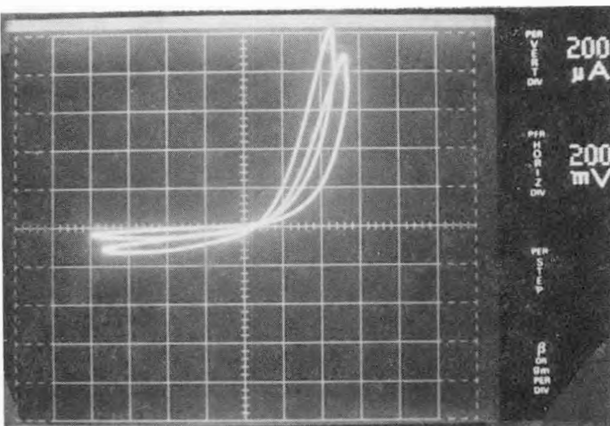

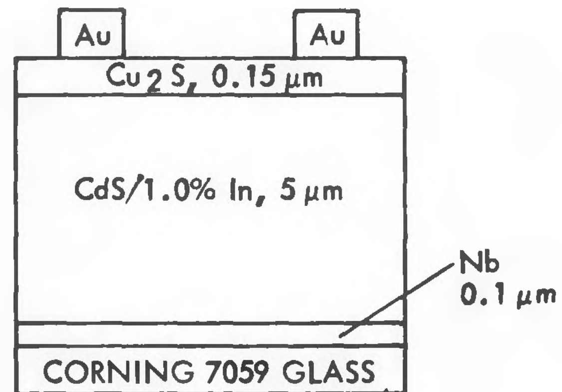

C. CELL #1194

Fig. 28 Single Grid Dark and AM 1 I-V Characteristics of As-Deposited Cells Prepared in Modified Deposition System

the pure CdS layer adjacent to the Cu_2S layer exhibits significant photovoltaic response ($I_{sc} \approx 0.1$ mA, $V_{oc} \approx 0.16$ V). Subsequent heat treatment of these cells resulted in no change in short circuit current and a maximum 25% increase in open-circuit voltage. It should be emphasized that these are very preliminary results with a new deposition system which is designed to provide improved control over deposition conditions. It is anticipated that this system will be able to reproduce the results previously obtained and that conditions will be established to produce cells of superior characteristics.

Section 4
CONCLUSION AND RECOMMENDATIONS

This report summarizes progress in the second year of a program to investigate the application of cylindrical-post-magnetron reactive sputtering to the production of solar-cell quality thin films of CdS/Cu_2S for terrestrial photovoltaic energy conversion. At the conclusion of the first year of the program, deposition condition — material parameter relationships were established and photovoltaic junctions demonstrated. During this second year of the program, photovoltaic device solar conversion efficiency improved from $\eta < 0.1\%$ to $\eta \approx 0.6\%$ for an all-sputter-deposited device. Table 4 summarizes recent work on sputtering as applied to the CdS/Cu_2S solar cell. The implication of this table is that the major problem is in characteristics of sputter-deposited CdS. Measurements on CdS films and Cu_2S/CdS devices as well as theoretical considerations applied to CdS and the reactive sputtering process tend to confirm the indirect evidence of Table 4.

As discussed in section 3.2, the all-sputtered Cu_2S/CdS cell illuminated I-V characteristic is dominated by the voltage dependence of junction collection efficiency. Reduction of S_I/μ and/or increase of E_o will cause an improvement in device I-V characteristics. These quantities are determined by the distribution of impurities and defects in the CdS. We have demonstrated a degree of control over material distribution in sputtered CdS films by fabrication and measurements in structures as shown in Fig. 19. Experiments to date indicate that an undoped In layer adjacent to the Cu_2S/CdS interface produces superior photovoltaic characteristics (Cell 653 in Fig. 1 and Cell 1181 in Fig. 28). It is expected that an undoped (Cd, Zn)S layer adjacent to the junction will result in further improvement through improved V_{oc}, reduced S_I/μ due to better lattice match to Cu_2S, and reduced impurity or dopant interdiffusion effects.

Section 5
REFERENCES

1. W. W. Anderson, A. D. Jonath, and J. A. Thornton, Cadmium Sulfide/Copper Sulfide Heterojunction Cell Research LMSC Final Report on Contract EG-77-C-03-1459 (Nov 1978)

2. A. Rothwarf, International Workshop on Cadmium Sulfide Solar Cells and Other Abrupt Heterojunctions, NSF-RANN AER 75-15858, University of Delaware, May 1975, pp 9 - 50

3. M. A. Lampert and P. Mark, Current Injection in Solids, Academic Press, New York, N. Y. 1970

4. J. Dieleman, International Workshop on Cadmium Sulfide Solar Cells and Other Abrupt Heterojunctions, NSF-RANN AER 75-15858, Univeristy of Delaware, May 1975, pp 92 - 107

5. L. R. Shiozawa, F. Augustine, G. A. Sullivan, J. M. Smith III and W. R. Cook, Jr., "Research on the Mechanism of the Photovoltaic Effect in High-Efficiency CdS Thin-Film Solar Cells", Contract AF33(615)-5334, ARL 69-0155, Oct 1969

6. A. Rothwarf, 2nd E. C. Photovoltaic Solar Energy Conference, ed. R. Van Overstraeten and W. Palz, D. Reidel Publishing Co., Dordrecht, 1979, pp 370 - 378

7. F. Guastavino, Contribution a l'etude des Properties Electriques et Optiques des Sulfures de Cuivre Cu_xS dans le Domaine 1, 75 x 2, 00 Thesis, Universite des Sciences et Techniques du Languedoc, Mar 1974

8. Lockheed Missile and Space Company, Inc., Cadmium Sulfide/Copper Sulfide Heterojunction Research, Technical Progress Report 3, Contract EG-77-C-03-1459 LMSC-D626523, Jun 1978

9. A. D. Jonath, W. W. Anderson, J. A. Thornton, and D. G. Cornog, J. Vac. Science and Technology 16, 200, 1979

10. B. J. Mulder, Phys. Status Solidi (a) 13, 79, 1972

11. J. A. Thornton, Cadmium Sulfide/Copper Sulfide Heterojunction Cell Research, Telic Corp. Tech. Progress Report 2, Contract XJ-9-8033-2, Nov 1979

12. W. W. Anderson, CdS/Cu_2S and CdS/Cu-Ternary Compund Program Contractors In-Depth Review Meeting, SERI, Wheatridge, CO, Dec 1979

13. C. A. Mead and W. G. Spitzer, Phys. Rev., 134, A713, 1964

14. D. L. Losee and E. L. Wolf, Phys. Rev., 187, 925, 1969

15. F. Gustavino, Contribution A L'Etude des Propriétés Electriques et Optiques des Sulfures de Cuivre Cu_xS dans le Domaine $1,75 < x < 2,00$. thesis submitted to the University of Science and Technology of Languedoc, Montpelier, France, 1974.

16. E. H. Roseboom, Jr., Econ. Geol. 61, 641 (1966)

17. W. R. Cook Jr., thesis, Case Western University, 1971

18. J. D. Meakin, et al. Cadmium Sulfide/Copper Sulfide Heterojunction Cell Research, Final Report on Contract EG-77-C-03-1576, May 1979

19. J. A. Thornton, "Cadmium Sulfide/Copper Sulfide Heterojunction Cell Research --Review of Telic work," Proceedings SERI CdS/Cu_2S and CdS/Cu Ternary Compound Review Mtg., Univ. of Delaware Feb. 28 - March 2, 1979.

20. V. Kumar and F. A. Kroger, "Self-Diffusion and Defect Structure of Cadmium Sulfide, "J. Solid State Chemistry, 3, 387 (1971)

21. R. H. Bube, Electronic Properties of Crystalline Solids, Academic Press, New York (1974) p. 310.

22. S. Wang, Solid State Eletronics, McGraw Hill, New York (1966), p. 178

23. W. Albers, Physical Chemistry of Defects," in Physics and Chemistry of II-VI Compounds, ed. by M. Aven and J. S. Prener, North-Holland, New York (1967), p. 165.

24. H. H. Woodbury, "Defect Characterization: Diffusivity and Electrical Measurement," II-IV Semiconducting Compounds, ed. by D. G. Thomas, Benjamin, New York (1967), p. 244

25. E. Nebauer, Physica Status Solidi 29, 269 (1968)

26. B. Gandham, R. Hill, H. A. Macleod and M. Bowden, Photovoltaic Solar Energy Conference, D. Reidel Publ. Co., Dordrecht, 1977, pp 1121-1130

27. M. J. Robertson and J. Woods, 2nd E. C. Photovoltaic Solar Energy Conference, ed. R. Van Overstraeten and W. Palz., D. Reidel Publ. Co., 1979, pp 909-916

28. N. C. Wyeth and A. Rothwarf, J. Vac. Sci. Technol. 16, 1402, 1979

29. T. S. TeVelde, Solid-State Electronics 16, 1305, 1973

30. L. D. Partain, G. A. Armantrout, J. Leong and P. Warter, Space-Charge-Limited Current in Cu_xS/CdS Solar Cells, Lawrence Livermore Laboratory Preprint UCRL-82883, 22 Jun 1979

31. J. W. Balch and W. W. Anderson, Physica Status Solidi (a) 9, 567, 1972

☆U.S. GOVERNMENT PRINTING OFFICE: 1980-740-145/639